

**NUMERICAL TECHNIQUES OF TSUNAMI SIMULATION
WITH SOURCE FAULT PLANE DATA AND MOVING
BOUNDARIES ON TRIANGULAR MESH**

(震源断層面データと三角形メッシュ上の移動境界
を伴う津波シミュレーションの数値的手法)

2018, September

NOVERINA ALFIANY

Graduate School of Environmental and Life Science
(Doctor's Course)
OKAYAMA UNIVERSITY

Abstract

Tsunami became an interesting subject to the researchers since its history and effects to the environment. To achieve a better understanding about the tsunamis behaviour, data from the past events in conjunction with theories and models should be employed. Aims of those studies are to predict and prepare a better countermeasure for the future tsunami events. Tsunami is a natural phenomena that causes severe damage and fatalities. Major tsunamis brought serious and widespread destructions. Studies of tsunami generation and propagation are essential. Earthquake or some other water bottom disturbances are the causative of tsunami generation. Those causative first generated the source fault plane of the initial tsunami wave, which at any time can collapse and approach coastal area.

This study was built on the numerical approach for the tsunami propagation. A nonlinear shallow water equation that is the system of partial differential equations was analyzed. The outcomes of numerical results contains information about tsunami characteristics and effects. Numerical techniques, specifically water elevation, were tested against the exact solutions of moving boundary shallow water equations. The initial water surface displacement based on source planes generated by other authors was set as an initial condition. A system of ordinary differential equations was obtained by reducing the system of partial differential equations with spatial discretization over a triangular mesh. Ordinary differential equations (ODE) solvers were applied in conjunction with a moving boundary technique. In the simulation, what is called, wet and dry scheme was applied at each time step. Our numerical techniques were utilized to simulate the Mentawai 2010 tsunami and the Indian Ocean 2004 tsunami.

The simulation of tsunami propagation at the Mentawai islands on October 25th, 2010 was carried out for the first 85 minutes. The wave heights at several points on Mentawai Island Regency were observed. The initial wave were generated from the source planes data and it produced the maximum water surface elevation approximately 3 m. The numerical results show that wave with heights up to 3 m occurred at a shoreline area of the South Pagai island, Mentawai Regency. Furthermore, the Indian Ocean tsunami 2004 was simulated for the first 1 hour. Most of the source fault planes have occurred in the vicinity of the Aceh Province area, among which the highest water surface displacement was up to 20 m. The maximum wave height up to 30 m was appeared at several points in the Aceh Province. Our numerical results were confirmed by some available data and other authors results.

Acknowledgement

In the name of ALLAH, The Most Gracious and Most Merciful

Greatest appreciation goes to Prof. Masaji Watanabe for the guidance, support, ideas, and motivation for almost three years of my studies. His supervision, taught, and patience made me a better researcher time to time. I am also grateful for the guidance of Prof. Tsuyoshi Kajiwara and Prof. Koji Kurihara during my studies.

The greatest thanks poured to my mother who always be there for me, and for my family. My best thanks goes to my sister Novrianti who always believe in me, no matter what. And for my friends and best friends.

This research was supported by a scholarship of the Ministry of Education, Culture, Sports, Science and Technology, Japan. The authors thank to Dr. Kazuhiro Yamamoto for his technical assistance. The results were generated by C computer programming language in conjunction with MATLAB programming platform and AVS/Express data visualization tool.

Contents

Abstract	i
Acknowledgement	ii
1 Introduction	1
1.1 Tsunami	1
1.2 Statement of the Problem	2
2 Mathematical Formulation	6
2.1 Shallow Water Equation	6
2.2 Numerical Formulation	8
2.3 Transformation to a Rectangular Coordinate	10
2.4 Okada Formulation	14
3 Numerical Techniques	17
3.1 Governing Equations	17
3.2 Discretization of Linearized Equations Over Triangular Mesh	18
3.3 Discretization of Governing Equations Over Triangular Mesh	19
4 Numerical Results	22
4.1 Verification of the Numerical Techniques	22
5 Numerical Simulation of Tsunami Propagation	26
5.1 The Algorithm of The Simulation	26
5.2 Simulation of the Mentawai 2010 Tsunami	28
5.3 Simulation of the Indian Ocean 2004 Tsunami	34
6 Conclusion and Future Research	43
6.1 Conclusions	43
6.2 Future Research	44
Bibliography	45

List of Figures

1.1	Tsunami wave illustration.	2
2.1	Triangular element e	9
2.2	The ellipsoid of the earth [21].	11
2.3	The visualization of the Mentawai bathymetry data.	13
2.4	Geometry of the source model [16].	15
2.5	The result of water surface deformation by Okada formula.	16
4.1	Profiles of the initial water surface.	24
4.2	Comparison of the water surface movement between numerical techniques (Green) and exact solutions (Blue).	25
5.1	An example of the 2D netCDF data sets display.	27
5.2	The illustration of the nodes and the elements numbering process.	28
5.3	The initial water surface displacement of 28 sub-faults [29].	29
5.4	The simulation of the initial water surface displacement.	29
5.6	Wave height changes at several points in the Mentawai Islands regency. . .	31
5.7	Wave height changes at Sipora islands in the Mentawai Islands regency. . .	31
5.8	Wave height changes at South Pagai islands in the Mentawai Islands Regency. .	32
5.9	Wave changes comparison between the Tanahbala station (red) and numerical results (green).	33
5.10	Wave changes comparison between the Teluk Dalam station (red) and numerical results (green).	33
5.11	Wave changes comparison between the Enggano station (red) and numerical results (green).	34
5.12	The initial water surface displacement of 22 sub-faults [30].	35
5.13	The initial water surface displacement of the Indian Ocean 2004 tsunami. . .	35
5.14	Wave height changes at several points in Aceh province, Indonesia.	36
5.15	Wave height transition at Banda Aceh in the Aceh province, Indonesia. . .	37
5.16	Wave height transition at Lampuuk beach in the Aceh province, Indonesia. .	37
5.17	Wave height transition at Aceh Jaya, Aceh province, Indonesia.	38
5.18	Wave height transition at Sabang in the Aceh province, Indonesia.	38
5.19	Wave height transition at Lhok Nga in the Aceh province, Indonesia. . . .	39
5.20	Wave height transition at Tapaktuan in the Aceh province, Indonesia. . . .	39
5.21	Wave height transition at Meulaboh in the Aceh province, Indonesia. . . .	40
5.5	Tsunami wave propagation of the Mentawai 2010 tsunami.	41
5.22	Tsunami wave propagation of the Indian Ocean 2004 tsunami [30].	42

List of Tables

1.1	The global largest moment magnitude per-millennium which produced tsunami [3].	3
1.2	The highest tsunami wave occurred in the Republic of Indonesia [3].	4
1.3	The list of the earthquakes occurred in the Sunda megathrust on period 2000-2010.	5

Chapter 1

Introduction

1.1 Tsunami

A wave is a change of the physical quantity which travel from the source area to other surrounding locations. Water wave is clasified according to the mechanism of a generation or based on the characteristics [1]. The causative factors and generating sources of a water wave include gravity, tide, wind, earthquake, landslide, iceberg collapses, and underwater volcanic activities, *etc.* Tsunami is a water wave that is generated mainly by an earthquake or underwater disturbance. Tsunami was classified as a long nonlinear wave which has a large amplitude. Tsunami wave occurs on the water surface with wave periods longer than minutes. At the time a tsunami wave reaches the shoreline, the wave height varies with the water depth.

Western Coastal and Marine Geology Institute [2] described the life circulation of tsunami wave as: (1) Underwater shaking pushes the water column up above mean sea level. Tsunami potential energy is transferred to the kinetic energy of the horizontal propagation. (2) The initial tsunami wave is generated within several minutes and travel towards the nearby coast. (3) The amplitude increases and the wave length decreases when approaching a shoreline. (4) A runup occurs immediately upon tsunami wave reached shoreline. The runup is a measurement of the water elevation above the mean sea level. (5) A part of the tsunami energy is reflected back to the ocean after runup.

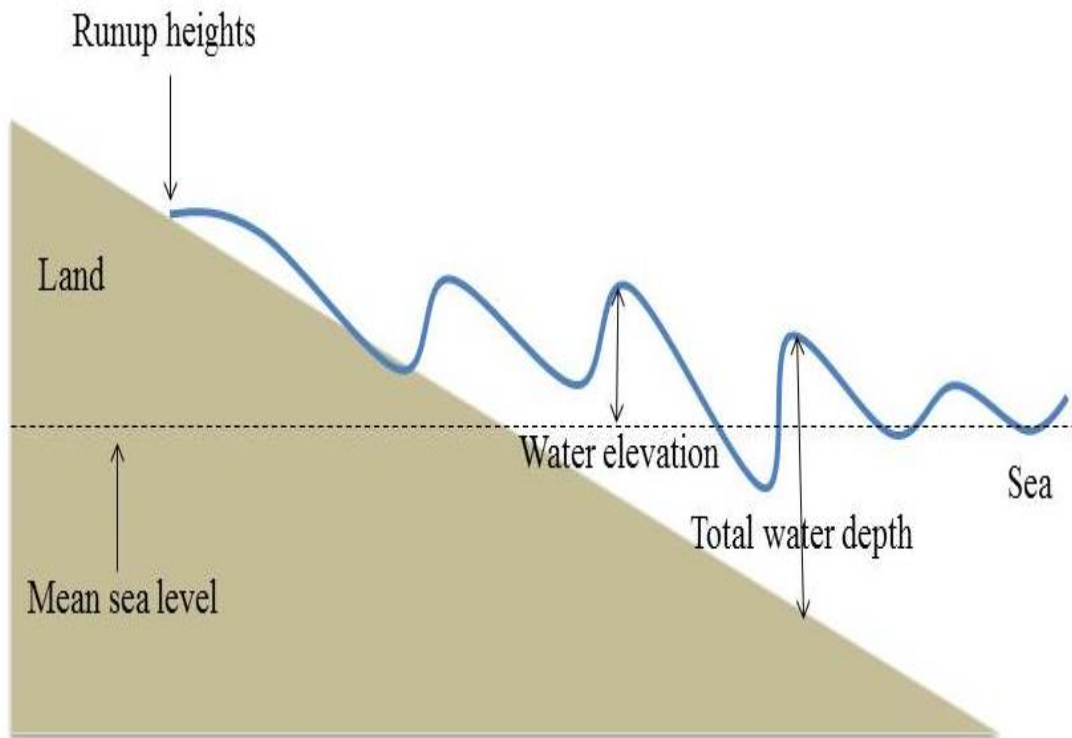


Figure 1.1: Tsunami wave illustration.

The National Centers for Environmental Information of National Oceanic and Atmospheric Administration (NOAA) noted that the first recorded tsunami event occurred on 2000 BC [3]. The unknown moment magnitude earthquake occurred at 35.800°E and 35.683°N , in the Syria coast area, Syria. The first known moment magnitude earthquake which produced a tsunami event was M_w 7.0, at the North Aegean, Greece. The earthquake occurred at 23.300°E and 39.700°N . The largest moment magnitude of an earthquake which produced a tsunami wave on the BC era was M_w 7.3, at the Corinthos-Patras Gulf, Greece. Table 1.1 describes the global tsunami events with the largest moment magnitude earthquake of each millenium period.

In the territory of Southeast Asia, the first recorded earthquake which generated a tsunami occurred at the Java Island coast, Indonesia, on 416 AD. The earthquake source was located at 105.423°E and 6.102°S . On July 1th, 1608 AD, another tsunami wave hit the Ternate Island, Indonesia, which was located at 127.352° longitude and 0.800° latitude. Table 1.2 describes the tsunami events with the maximum wave height greater than ten meters in the Indonesia region.

1.2 Statement of the Problem

The Sumatra island is a part of Greater Sunda Islands archipelago. This island is located at 102°E and 0°N and known as the largest island in the Republic of Indonesia. Sumatra

Source: National Centers for Environmental Information, NOAA website.

No.	Periode	Year	Moment Magnitude (M_w)	Location	Maximum Wave Height (m)
1	2nd millenium BC	unknown	unknown	unknown	unknown
2	1st millenium BC	373	7.3	Corinthos-Patras Gulf, Greece	unknown
3	1st millenium AD	869	8.6	Sanriku, Japan	-
		887	8.6	Nankaido, Japan	-
4	2nd millenium AD	1960	9.5	Southern Chile, Chile	25.00
5	3rd millenium AD	2004	9.1-9.3	Off west coast of Sumatra, Indonesia	50.90
		2011	9.1	Honshu Island, Japan	38.90

Table 1.1: The global largest moment magnitude per-millenium which produced tsunami [3].

Island has a strike-slip fault (the Great Sumatran fault) which is stretching out on the entire length of the island, and a subduction zone (the Sunda megathrust) is the most seismogenic structures on the earth. A strike-slip fault is a fault plane on which rock strata are displaced mainly in a horizontal direction, parallel to the line of the fault plane. The Great Sumatran fault zone accomodates most of the strike-slip motion between the Indo-Australian plate and the Eurasian plate. A subduction is a destructive plate boundaries of tectonic plates. In this process the movement of one plate below another is forced or sinks due to gravity. A subduction zone is a region where this process occurs. In particular, the Sunda megathrust was responsible for many earthquakes in the Indonesia.

Table 1.3 lists the earthquakes due to geological processes of the Sunda megathrust at Sumatra Island with the moment magnitude M_w greater than seven. Seven out of the thirteen earthquakes were produced tsunami waves that caused serious disasters. The most recent most devastating tsunami event in the Sunda megathrust region was the Indian Ocean tsunami which occured on December 26th, 2004. The Indian Ocean 2004 earthquake recorded the third largest magnitude millenium AD. Studies estimated the moment magnitude (M_w) of the earthquake between 9.1 and 9.3. The tsunami generated by this earthquake was the most devastating and deadly one, with more than 200,000 fatalities along the coasts of the Indian Ocean [5]. An earthquake with moment magnitude M_w 7.8 and epicenter 20 km below the surface occured at Mentawai Island Recency, Indonesia on October 25th, 2010. The Mentawai Islands earthquake generated the much larger tsunami than expected from its seismic magnitude [6]. The maximum tsunami wave height 16.90 m was produced by the Mentawai Islands 2010 earthquake. This event caused 435 casualties and hundreds of people vanished from the entire Mentawai Islands regency.

A recent explication shows that Indonesia, especially the Sumatra Island is the high risk region of the tsunami event. The high numbers of fatalities due to the tsunami attack generally caused by the lack of comprehension or the unavailability of tsunami early warning system. A tsunami wave are described mathematically as a system of linear or nonlinear partial differential equations. Those system of partial differential equations can be solved numerically to simulate tsunami wave propagation. A simulation illustrates tsunami wave generation and propagation. Numerical studies of tsunami generation and

Source: National Centers for Environmental Information, NOAA website.

No.	Date	Moment Magnitude (M_w)	Location	Coordinate	Maximum Wave Height (m)
1	August 1 th , 1629	-	Banda Sea	129.900°E, 4.600°S	16.00
2	February 17 th , 1674	6.8	Banda Sea	127.750°E, 3.750°S	100.00
3	1799	-	Southeast Sumatra	101.000°E, 2.000°S	15.00
4	December 29 th , 1820	7.5	Flores Sea	119.000°E, 7.000°S	25.00
5	June 28 th , 1859	7.0	North Moluccas Islands	126.500°E, 1.000°N	10.00
6	March 3 rd , 1871	-	Ruang	125.425°E, 2.280°S	25.00
7	August 27 th , 1883	-	Krakatau	105.423°E, 6.102°S	41.00
8	September 29 th , 1899	7.8	Banda Sea	128.500°E, 3.000°S	12.00
9	December 1 th , 1927	6.3	Sulawesi	119.700°E, 0.700°S	15.00
10	August 4 th , 1928	-	Flores Sea	121.708°E, 8.320°S	10.00
11	March 17 th , 1930	-	Krakatau	105.423°E, 6.102°S	500.00
12	August 22 nd , 1968	7.8	Banda Sea	119.800°E, 0.200°N	10.00
13	December 12 th , 1992	7.8	Flores Sea	121.896°E, 8.480°S	26.20
14	June 2 nd , 1994	7.8	South of Java	112.835°E, 10.477°S	13.90
15	December 26 th , 2004	9.1	Off west coast of Sumatra	95.854°E, 3.316°N	50.90
16	July 17 th , 2006	7.7	South of Java	107.411°E, 9.254°S	20.90
17	October 25 th , 2010	7.7	Mentawai Islands, Sumatra	100.082°E, 3.487°S	16.90

Table 1.2: The highest tsunami wave occurred in the Republic of Indonesia [3].

propagation can provide sufficient outcomes to described tsunami characteristics and effects. Those outcomes can lead to the establishment of a tsunami hazard assessment and a tsunami early warning system.

Poisson, *et.al.* [7] simulated the Indian Ocean 2004 tsunami by the tsunami code Geowave at the eastern coast of Sri Lanka. The Geowave model was based on fully nonlinear Boussinesq equations. The simulation was induced by five different models of the seismic source. They made a comparison between the simulation results and the satellite Jason-1 data. A numerical simulation was based on the 3-dimensional shallow water equations [8]. A nonlinear dispersive Reynolds-averaged Navier-Stokes equations were studied by using the FLOW3D code to simulate the coastal runoff behavior at the Lhok Nga, Aceh. The tsunami source fault plane parameters proposed by Tanioka, *et.al* [9] were utilized. A number of numerical simulations were performed by Syamsidik, *et.al.* [10]. The simulations were based on the Cornell Multi-grid Coupled Tsunami (COMCOT) model. The data were obtained from the Indian Ocean 2004 tsunami event and a future near-shore tsunami events around the Mentawai Island.

The Mentawai Island 2010 tsunami was simulated based on the shallow water equations [11]. Two numerical models were employed and performed by using nonlinear and dispersive long wave tsunami models (TUNAMI N” and SWAN). A tsunami simulation system which was an integration part of the Global Disasters Alerts and Coordinate System (GDACS) established by Ulutas, *et.al.* [12]. This study aims to assess the tsunami hazard on the Mentawai and Sumatra coast. Satake, *et.al.* [6] simulated tsunami wave heights of the Mentawai 2010 using linear computations on a spherical coordinate sys-

Source: NOAA and USGS website [3],[4].

No.	Date	Time (UTC)	Location	Coordinate	Moment Magnitude (M_w)	Result
1	June 4 th , 2000	4:21:16	Enggano, Bengkulu	102.087°E, 4.721°S	7.9	-
2	November 2 nd , 2002	1:26:10	Simeulue, Aceh	96.085°E, 2.824°N	7.3	-
3	December 26 th , 2004	0:58:53	Off west coast of Aceh	95.854°E, 3.316°N	9.1-9.3	Tsunami
4	March 28 th , 2005	16:9:36	Southwest Sumatra	97.108°E, 2.085°N	8.6	Tsunami
5	September 12 th , 2007	11:10:26	Bengkulu	101.367°E, 4.438°S	8.4	Tsunami
	September 12 th , 2007	23:49:3	Bengkulu	100.841°E, 2.625°S	7.9	-
6	September 13 th , 2007	3:35:26	Padang, West Sumatra	99.851°E, 2.160°S	7.0	-
7	February 20 th , 2008	8:8:30	Banda Aceh, Aceh	95.964°E, 2.768°N	7.4	-
8	February 25 th , 2008	8:36:33	Padang, West Sumatra	99.972°E, 2.486°S	7.2	Tsunami
9	September 30 th , 2009	10:16:9	Padang, West Sumatra	99.867°E, 0.720°S	7.6	Tsunami
10	April 6 th , 2010	22:15:1	Medan, North Sumatra	97.048°E, 2.383°N	7.8	Tsunami
11	May 9 th , 2010	5:59:41	Simeulue Island, Aceh	96.018°E, 3.748°N	7.2	-
12	October 25 nd , 2010	14:42:22	Mentawai, West Sumatra	100.082°E, 3.487°S	7.7	Tsunami

Table 1.3: The list of the earthquakes occurred in the Sunda megathrust on period 2000-2010.

tem and a system of nested grids. A finite difference scheme in the Cartesian coordinate system was used to solved the nonlinear shallow water equations to simulated the wave heights.

In this study, the nonlinear shallow water equations based on [13] were analyzed numerically by using finite element analysis to simulated the Indian Ocean 2004 tsunami and the Mentawai 2010 tsunami. A governing equations is a system of partial differential equations derived from momentum equations and a continuity equation. Furthermore, the system of partial differential equations was spatially discretized for reduction to a system of ordinary differential equations (ODE) over a triangular mesh. The ODE solvers were applied to the resultant of the system of ODE's in conjunction with a moving boundary technique. The numerical techniques were tested by comparing the numerical results againsts the exact solutions of the two-dimensional nonlinear shallow water equations involving linear bottom friction for flow above parabolic bottom topography [14, 15]. The seafloor vertical deformation of those tsunami events were computed by using Okada formulation [16, 17] based on the source faults plane parameters. The results of the computation were set as an initial water surface displacement for tsunami simulation. The simulation and wave height changes of the Indian Ocean 2004 tsunami and the Mentawai 2010 tsunami were illustrated.

Chapter 2

Mathematical Formulation

2.1 Shallow Water Equation

In the theory of a long wave, the vertical acceleration of water particles are negligible except for an oceanic propagation of tsunami [13]. The vertical motion of water particles has small effect on the water pressure distribution in consequence of the negligibility of the vertical acceleration compared to the gravitational acceleration. The approximation of the pressure distribution, with the hydrostatic pressure and the negligibility of the vertical acceleration lead to by equations (2.1)-(2.4). The equations of mass conservation and momentum in the three dimensional problem are expressed by

$$\frac{\partial \eta}{\partial t} + \frac{\partial u}{\partial x} + \frac{\partial v}{\partial y} + \frac{\partial w}{\partial z} = 0, \quad (2.1)$$

$$\frac{\partial u}{\partial t} + u \frac{\partial u}{\partial x} + v \frac{\partial u}{\partial y} + w \frac{\partial u}{\partial z} + \frac{1}{\rho} \frac{\partial p}{\partial x} + \frac{1}{\rho} \left(\frac{\partial \tau_{xx}}{\partial x} + \frac{\partial \tau_{xy}}{\partial y} + \frac{\partial \tau_{xz}}{\partial z} \right) = 0, \quad (2.2)$$

$$\frac{\partial v}{\partial t} + u \frac{\partial v}{\partial x} + v \frac{\partial v}{\partial y} + w \frac{\partial v}{\partial z} + \frac{1}{\rho} \frac{\partial p}{\partial y} + \frac{1}{\rho} \left(\frac{\partial \tau_{xy}}{\partial x} + \frac{\partial \tau_{yy}}{\partial y} + \frac{\partial \tau_{yz}}{\partial z} \right) = 0, \quad (2.3)$$

$$g + \frac{1}{\rho} \frac{\partial \rho}{\partial z} = 0. \quad (2.4)$$

Let η be the vertical displacement above the still water surface. The functions u , v , and w are the water particle velocities in the x -, y -, and z -direction, respectively, where x and y are the horizontal axis while z is the vertical axis. The constant g is the gravitational acceleration, ρ is the water density, and τ_{ij} is the normal or tangential shear stress in the i direction on the j normal plane. The variable p is the hydrostatic pressure.

The dynamic and kinetic conditions at the surface and the bottom are given by

$$p = 0 \text{ at } z = \eta, \quad (2.5)$$

$$w = \frac{\partial \eta}{\partial t} + u \frac{\partial \eta}{\partial x} + v \frac{\partial \eta}{\partial y} \text{ at } z = \eta, \quad (2.6)$$

$$w = -u \frac{\partial h}{\partial x} - v \frac{\partial h}{\partial y} \text{ at } z = -h. \quad (2.7)$$

The Leibniz rule is applied to the equations (2.1)-(2.4). The dynamic and kinetic conditions (2.5)-(2.7) were used, and the two-dimensional shallow water equations was obtained.

$$\frac{\partial \eta}{\partial t} + \frac{\partial M}{\partial x} + \frac{\partial N}{\partial y} = 0, \quad (2.8)$$

$$\frac{\partial M}{\partial t} + \frac{\partial}{\partial x} \left(\frac{M^2}{H} \right) + \frac{\partial}{\partial y} \left(\frac{MN}{H} \right) + gH \frac{\partial \eta}{\partial x} + \frac{\tau_x}{\rho} = A \left(\frac{\partial^2 M}{\partial x^2} + \frac{\partial^2 M}{\partial y^2} \right), \quad (2.9)$$

$$\frac{\partial N}{\partial t} + \frac{\partial}{\partial x} \left(\frac{MN}{H} \right) + \frac{\partial}{\partial y} \left(\frac{N^2}{H} \right) + gH \frac{\partial \eta}{\partial y} + \frac{\tau_y}{\rho} = A \left(\frac{\partial^2 N}{\partial x^2} + \frac{\partial^2 N}{\partial y^2} \right). \quad (2.10)$$

Here $H = h + \eta$ is the total water depth. The variable A is the horizontal eddy viscosity which assumed to be constant in space. The variables M and N are the discharge fluxes in the x -direction and y -direction, respectively, that is

$$M = \int_{-h}^{\eta} u \, dz \approx u(h + \eta) = uH, \quad (2.11)$$

$$N = \int_{-h}^{\eta} v \, dz \approx v(h + \eta) = vH. \quad (2.12)$$

The terms τ_x and τ_y are the bottom frictions in the x -direction and y -direction, respectively.

$$\frac{\tau_x}{\rho} = \frac{1}{2g} \frac{f}{H^2} M \sqrt{M^2 + N^2}, \quad \frac{\tau_y}{\rho} = \frac{1}{2g} \frac{f}{H^2} N \sqrt{M^2 + N^2}. \quad (2.13)$$

The variable f is the friction coefficient in conjunction of Manning's roughness n , written by

$$n = \sqrt{\frac{fH^{\frac{1}{3}}}{2g}}. \quad (2.14)$$

Thus the bottom friction became

$$\frac{\tau_x}{\rho} = \frac{fn^2}{H^{\frac{7}{3}}} M \sqrt{M^2 + N^2}, \quad \frac{\tau_y}{\rho} = \frac{fn^2}{H^{\frac{7}{3}}} N \sqrt{M^2 + N^2}. \quad (2.15)$$

Equations (2.16)-(2.18) were obtained by neglecting the horizontal eddy turbulence viscosity A . The term eddy in fluid dynamics refer to the swirling of a fluid and the reverse current. Eddy is created when the fluid is in a turbulent flow regime. Whereas, the term turbulence is any pattern of fluid motion characterized by changes in pressure and flow

velocity. Those equations (2.16)-(2.18) are a model for the propagation of tsunami wave in the shallow water consisting the bottom friction.

$$\frac{\partial \eta}{\partial t} + \left(\frac{\partial M}{\partial x} + \frac{\partial N}{\partial y} \right) = 0, \quad (2.16)$$

$$\frac{\partial M}{\partial t} + \frac{\partial}{\partial x} \left(\frac{M^2}{H} \right) + \frac{\partial}{\partial y} \left(\frac{MN}{H} \right) + gH \frac{\partial \eta}{\partial x} + \frac{gn^2}{H^{\frac{7}{3}}} M \sqrt{M^2 + N^2} = 0, \quad (2.17)$$

$$\frac{\partial N}{\partial t} + \frac{\partial}{\partial x} \left(\frac{MN}{H} \right) + \frac{\partial}{\partial y} \left(\frac{N^2}{H} \right) + gH \frac{\partial \eta}{\partial y} + \frac{gn^2}{H^{\frac{7}{3}}} N \sqrt{M^2 + N^2} = 0. \quad (2.18)$$

Equations (2.16)-(2.18) are the governing equations for our numerical scheme for simulating the tsunami wave propagation.

2.2 Numerical Formulation

The domain in the xy -plane is subdivided into triangular elements with the total number of nodes m and total number of elements l . The element with a triangle shape is the most widely used in finite element analysis. A basis function associated with the i^{th} node is a piecewise linear continuous function. A piecewise linear function ϕ_j which satisfies $\phi_j(x_i, y_i) = \delta_{ij}$ will be derived for the triangular elements. Let a linear case polynomial is used to interpolate a function u associated to two-dimensional coordinate (x, y) , given by [18]

$$u(x, y) = \alpha_1 + \alpha_2 x + \alpha_3 y. \quad (2.19)$$

Here, α_1 , α_2 , and α_3 are the constants.

Suppose that (x_i, y_i) , (x_j, y_j) , and (x_k, y_k) are the coordinate of nodes i , j , and k of element e , respectively. The interpolation function u associated nodes i , j , and k is expressed by

$$u(x_i, y_i) = \alpha_1 + \alpha_2 x_i + \alpha_3 y_i, \quad (2.20)$$

$$u(x_j, y_j) = \alpha_1 + \alpha_2 x_j + \alpha_3 y_j, \quad (2.21)$$

$$u(x_k, y_k) = \alpha_1 + \alpha_2 x_k + \alpha_3 y_k. \quad (2.22)$$

Those functions are satisfies the conditions

$$u(x_i, y_i) = u_i, u(x_j, y_j) = u_j, u(x_k, y_k) = u_k, \quad (2.23)$$

where u_i , u_j , and u_k are the values of $u(x, y)$ at the vertices i , j , and k , respectively.

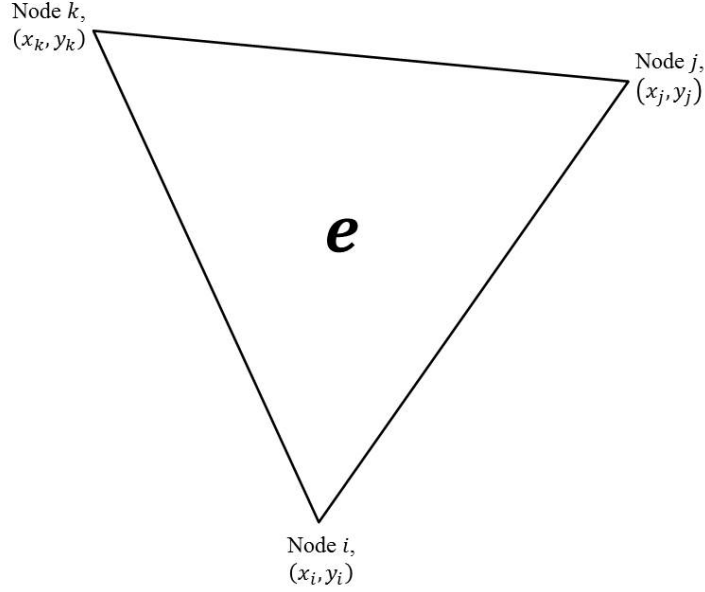


Figure 2.1: Triangular element e .

The value of function $u(x, y)$ for element e (Fig. 2.1) is expressed by [19]

$$u(x, y) = u_i \phi_i^{(e)}(x_i, y_i) + u_j \phi_j^{(e)}(x_j, y_j) + u_k \phi_k^{(e)}(x_k, y_k). \quad (2.24)$$

Here, $\phi_i^{(e)}$, $\phi_j^{(e)}$, and $\phi_k^{(e)}$ are the piecewise linear functions for the triangular element, given by

$$\phi_i^{(e)} = \frac{1}{2A_e}(\alpha_{i1} + \alpha_{i2}x_i + \alpha_{i3}y_i), \quad (2.25)$$

$$\phi_j^{(e)} = \frac{1}{2A_e}(\alpha_{j1} + \alpha_{j2}x_j + \alpha_{j3}y_j), \quad (2.26)$$

$$\phi_k^{(e)} = \frac{1}{2A_e}(\alpha_{k1} + \alpha_{k2}x_k + \alpha_{k3}y_k). \quad (2.27)$$

Here, A_e is the area of the triangle e which given by

$$A_e = \frac{x_i(y_j - y_k) + x_j(y_k - y_i) + x_k(y_i - y_j)}{2}. \quad (2.28)$$

Constants α_{i1} , α_{i2} , and α_{i3} are expressed by

$$\alpha_{i1} = x_j y_k - x_k y_j, \alpha_{i2} = y_j - y_k, \alpha_{i3} = x_k - x_j. \quad (2.29)$$

Index i , j , and k satisfies $i \neq j \neq k$ and i , j , k are changes order on clockwise direction. Thus, the piecewise function $\phi_j^{(e)}(x_i, y_i)$ is given by

$$\phi_j^{(e)}(x_i, y_i) = \begin{cases} 1 & \text{if } i = j \\ 0 & \text{if } i \neq j \end{cases}. \quad (2.30)$$

The partial derivatives of approximation (2.24) for any function u with respect to x and y is expressed with

$$\frac{\partial u}{\partial x} = u_i \frac{y_j - y_k}{2A_e} + u_j \frac{y_k - y_i}{2A_e} + u_k \frac{y_i - y_j}{2A_e}, \quad (2.31)$$

$$\frac{\partial u}{\partial y} = u_i \frac{x_k - x_j}{2A_e} + u_j \frac{x_i - x_k}{2A_e} + u_k \frac{x_j - x_i}{2A_e}. \quad (2.32)$$

The approximate value of $\frac{\partial u}{\partial x}$ and $\frac{\partial u}{\partial y}$ at the i^{th} node, are the weighted average value of their partial derivations over the element which shared the same node i .

$$\left(\frac{\partial u}{\partial x}\right)_i = \frac{1}{\sum_{k=1}^l (A_e)_k} \sum_{k=1}^l (A_e)_k \left(\frac{\partial u}{\partial x}\right)^{(k)}, \quad (2.33)$$

$$\left(\frac{\partial u}{\partial y}\right)_i = \frac{1}{\sum_{k=1}^l (A_e)_k} \sum_{k=1}^l (A_e)_k \left(\frac{\partial u}{\partial y}\right)^{(k)}. \quad (2.34)$$

Here, $\left(\frac{\partial u}{\partial x}\right)^{(k)}$ and $\left(\frac{\partial u}{\partial y}\right)^{(k)}$ are the approximate value of the partial derivative $\left(\frac{\partial u}{\partial x}\right)_i$ and $\left(\frac{\partial u}{\partial y}\right)_i$ in the k -th element, respectively.

2.3 Transformation to a Rectangular Coordinate

The Gauss-Krug er projection is a mapping of a coordinate reference ellipsoid of the earth onto a plane coordinate, where the equator and central meridian remain as straight lines and the scale along the central meridian is constant [20]. The ellipsoid is a surface of revolution created by rotating an ellipse about its minor axis. Fig. 2.2 shows an ellipsoid with center O , the rotation axis north-south NS , and the equatorial plane EAE' [21]. The segment $OA = OE = a$ is the major radius of the ellipsoid, and $ON = b$ is the minor radius. The geometrical constants of the ellipsoid are given by

$$f = \frac{a - b}{a}, \quad e = \sqrt{\frac{a^2 - b^2}{a^2}}, \quad e' = \sqrt{\frac{a^2 - b^2}{b^2}}, \quad e^2 = \frac{e'^2}{1 + e'^2}, \quad e'^2 = \frac{e^2}{1 - e^2}. \quad (2.35)$$

Here f is the flattening constant, e and e' are the first eccentricity and the 2nd eccentricity, respectively.

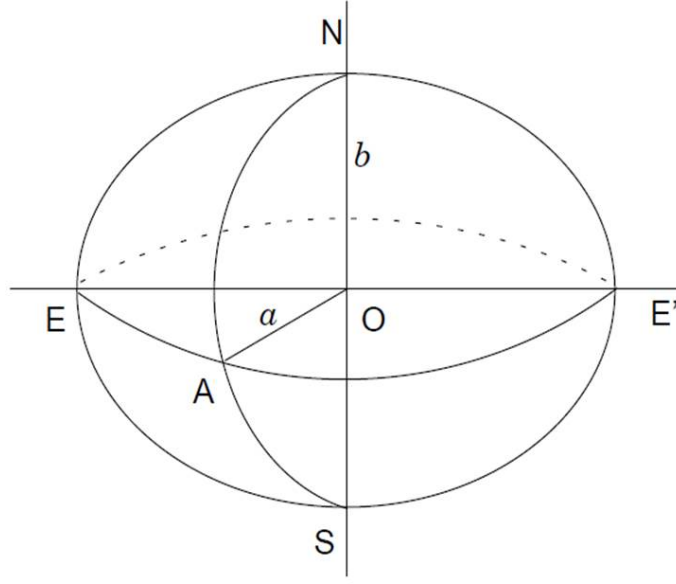


Figure 2.2: The ellipsoid of the earth [21].

The value of the major radius is given by $a = 6378137.0$ m and the value of the flattening constant is given by $f = \frac{1}{298.257223563}$. The meridian curvature radius M is the arc of the meridian. Its measured from the equator to the point of latitude φ .

$$M = \frac{a(1 - e^2)}{(1 - e^2 \sin^2 \varphi)^{\frac{3}{2}}}, \quad (2.36)$$

where φ is the curvilinear coordinate latitude. The radius of the curvature N ,

$$N = \frac{a}{\sqrt{1 - e^2 \sin^2 \varphi}} = \frac{a^2}{\sqrt{a^2 \cos^2 \varphi + b^2 \sin^2 \varphi}}. \quad (2.37)$$

Parameter R is the average of the curvature radius

$$R = \sqrt{MN}. \quad (2.38)$$

The Gauss-Krugër projection converts the curvilinear coordinates to (x, y) coordinate. Furthermore, the (x, y) coordinate plane converted to (X, Y) coordinate plane. Here, x and X represent the length in the north-south NS (latitude) direction, and y and Y represent the direction in the east-west EW (longitude) direction. Consider the derivative ds of the arc of a meridian ellipse. The derivative is a circle of the meridian curvature radius M . Let M is the length of the arc of $d\varphi$, expressed by

$$ds = \frac{a(1 - e^2)}{(1 - e^2 \sin^2 \varphi)^{\frac{3}{2}}} d\varphi. \quad (2.39)$$

The length of the arc between two points latitude φ_1 and φ_2 is

$$s = \int_{\varphi_1}^{\varphi_2} \frac{a(1 - e^2)}{(1 - e^2 \sin^2 \varphi)^{\frac{3}{2}}} d\varphi. \quad (2.40)$$

The integration by using series expansion is utilized

$$s = B - B_0. \quad (2.41)$$

Here B is the measurement meridian arc length, given by

$$B = a(1 - e^2) \left[A' \varphi_2 - \frac{B'}{2} \sin 2\varphi_2 + \frac{C'}{4} \sin 4\varphi_2 - \frac{D'}{6} \sin 6\varphi_2 + \frac{E'}{8} \sin 8\varphi_2 - \frac{F'}{10} \sin 10\varphi_2 + \dots \right], \quad (2.42)$$

where B_0 expressed by

$$B_0 = a(1 - e^2) \left[A' \varphi_1 - \frac{B'}{2} \sin 2\varphi_1 + \frac{C'}{4} \sin 4\varphi_1 - \frac{D'}{6} \sin 6\varphi_1 + \frac{E'}{8} \sin 8\varphi_1 - \frac{F'}{10} \sin 10\varphi_1 + \dots \right]. \quad (2.43)$$

The constants A' , B' , C' , D' , E' , and F' are given by

$$A' = 1 + \frac{3}{4}e^2 + \frac{45}{64}e^4 + \frac{175}{256}e^6 + \frac{11025}{16384}e^8 + \frac{43659}{65536}e^{10}, \quad (2.44)$$

$$B' = \frac{3}{4}e^2 + \frac{15}{16}e^4 + \frac{525}{512}e^6 + \frac{2205}{2048}e^8 + \frac{72765}{65536}e^{10}, \quad (2.45)$$

$$C' = \frac{15}{64}e^4 + \frac{105}{256}e^6 + \frac{2205}{4096}e^8 + \frac{10395}{16384}e^{10}, \quad (2.46)$$

$$D' = \frac{35}{512}e^6 + \frac{315}{2048}e^8 + \frac{31185}{131072}e^{10}, \quad (2.47)$$

$$E' = \frac{315}{16384}e^8 + \frac{3465}{65536}e^{10}, \quad (2.48)$$

$$F' = \frac{693}{131072}e^{10}. \quad (2.49)$$

Let λ_0 is the longitude as the origin of the curvilinear coordinate when converting the ellipsoid coordinate of an arbitrary point. Considering the transformation of (λ, φ) into the plane coordinate (x, y) , and

$$l = \lambda - \lambda_0. \quad (2.50)$$

The transformation formula of (λ, φ) to (x, y) is given by

$$\begin{aligned} x = B + \frac{Nl^2}{2} \sin \varphi \cos \varphi + \frac{Nl^4}{24} \sin \varphi \cos^3 \varphi (5 - t^2 + 9\eta^2 + 4\eta^4) \\ + \frac{Nl^6}{720} \sin \varphi \cos^5 \varphi (61 - 58t^2 + t^4 + 270\eta^2 - 330t^2\eta^4) \\ + \frac{Nl^8}{40320} \sin \varphi \cos^7 \varphi (1385 - 3111t^2 + 543t^4 - t^6) + \dots, \end{aligned} \quad (2.51)$$

$$\begin{aligned}
y &= Nl \cos \varphi + \frac{Nl^3}{6} \cos^3 \varphi (1 - t^2 + \eta^2) \\
&+ \frac{Nl^5}{120} \cos^5 \varphi (5 - 18t^2 + t^4 + 14\eta^2 - 58t^2\eta^2) \\
&+ \frac{Nl^7}{5040} \cos^7 \varphi (61 - 479t^2 + 179t^4 - t^6) + \dots
\end{aligned} \tag{2.52}$$

Here, $t = \tan \varphi$, $\eta^2 = e'^2 \cos^2 \varphi$, N is the radius of the curvature, and M is the radius of the meridian curvature. Note that the converted x is in the north-south direction and y is in the east-west direction.

A formula to convert the (x, y) coordinate into the coordinate (X, Y) is given by

$$X = m_0 k (x - B_0) + X_0, \tag{2.53}$$

$$Y = m_0 k y + Y_0. \tag{2.54}$$

Here m_0 is a meridian where longitude defined as zero (0°), B_0 is the meridian from the equator to the origin latitude of the plane coordinate system. Coefficient k given by

$$k = 1 + \frac{h_0}{r_0}, \quad r_0 = \sqrt{M_0 N_0}, \tag{2.55}$$

where h_0 is the height of the coordinate plane from the ellipsoid plane and r_0 is the average radius of curvature of the origin, obtained by equation (2.38). Those projection are utilized to transform our bathymetry data into (X, Y) coordinate. Fig. 2.3 shows the visualization of the Mentawai bathymetry data transformed by the previous Gauss-Kruger projection.

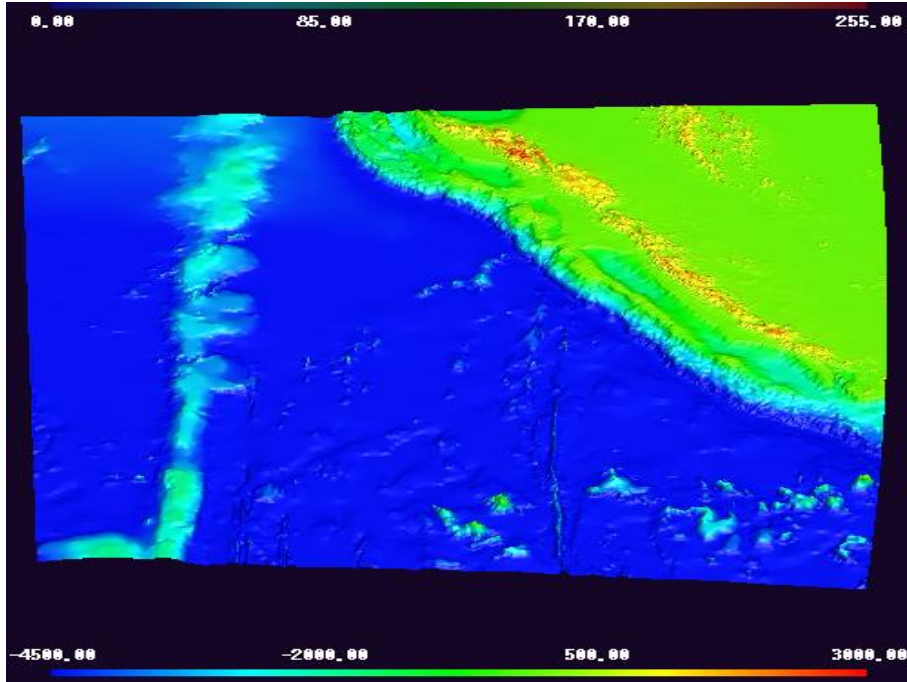


Figure 2.3: The visualization of the Mentawai bathymetry data.

2.4 Okada Formulation

Okada formulation is a model to calculate the displacement of water surface u_i and its spatial derivative $\frac{\partial u_i}{\partial x_j}$ at an arbitrary point. It gives the displacement at an arbitrary point on the surface or inside of the semi-infinite medium due to a point source or a finite rectangular fault [16,17]. The deformation field $u_i(x_1, x_2, x_3)$ due to a dislocation $\Delta u_j(\xi_1, \xi_2, \xi_3)$ over a surface Σ for a point source is given by

$$u_i = \frac{1}{F} \int \int_{\Sigma} \Delta u_j \left[\lambda \delta_{jk} \frac{\partial u_i^n}{\partial \xi_n} + \mu \left(\frac{\partial u_i^j}{\partial \xi_k} + \frac{\partial u_i^k}{\partial \xi_j} \right) \right] v_k d\Sigma, \quad (2.56)$$

where δ_{jk} is the Kronecker delta, λ and μ are Lamé's constants, v_k is the direction cosine of the normal to the surface element $d\Sigma$. The function ∂u_i^j is the i -th component of the displacement at (x_1, x_2, x_3) due to the j -th direction point force of magnitude F at (ξ_1, ξ_2, ξ_3) [16]. The coordinate (ξ_1, ξ_2, ξ_3) is the coordinate of the point on the surface, and (x_1, x_2, x_3) is the coordinate of the observation point. The displacement $u_i(x_1, x_2, x_3)$ is considered in an isotropic medium. An isotropic medium is an object or substance which having a physical property that has the same value when measured in the different directions. The dislocation is the distance of a relative motion between fault plane.

A calculation of the strain and stress in the medium expressed as

$$\varepsilon_{ij} = \frac{1}{2} \left(\frac{\partial u_i}{\partial x_j} + \frac{\partial u_j}{\partial x_i} \right), \quad (2.57)$$

$$\tau_{ij} = \lambda \varepsilon_{kk} \delta_{ij} + 2\mu \varepsilon_{ij}. \quad (2.58)$$

The Cartesian coordinate system (Fig. 2.4) is utilized. The medium occupies the region of $z \leq 0$. Axis x is taken to be parallel to the strike fault (U_1) direction. The dislocations U_1 , U_2 , and U_3 are define as the strike-slip, dip-slip, and tensile components of dislocation. A strike-slip is the nearly vertical fractures where the blocks have mostly moved horizontally. A dip-slip is the inclined fractures where the blocks have mostly shifted vertically. A tensile is the force required to pull something to the point where it breaks. The location of the point source is $(0, 0, -d)$.

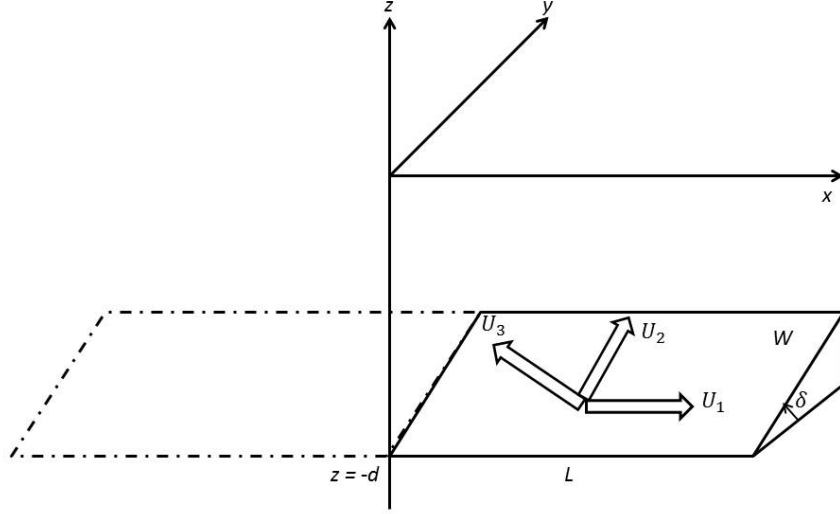


Figure 2.4: Geometry of the source model [16].

For a finite rectangular fault source with length L and width W , the deformation field can be derived by taking

$$x = x - \varepsilon', \quad y = y - \eta' \cos(\delta), \quad d = d - \eta' \sin(\delta). \quad (2.59)$$

The integration

$$\int_x^{x-L} d\varepsilon \int_p^{p-L} d\eta, \quad (2.60)$$

was performed, where $x - \varepsilon' = \varepsilon$, $p - \eta' = \eta$, and $p = y \cos \delta + d \sin \delta$. The substitution

$$f(\varepsilon, \eta) \equiv f(x, p) - f(x, p - W) - f(x - L, p) + f(x - L, p - W), \quad (2.61)$$

is used to obtain the displacement field in a rectangular fault source.

The surface deformation corresponding to x , y , and z components is given by

$$\mathbf{u}(x, y, 0) = \mathbf{u}_B(x, y, 0), \quad (2.62)$$

$$\frac{\partial \mathbf{u}}{\partial x}(x, y, 0) = \frac{\partial \mathbf{u}_B}{\partial x}(x, y, 0), \quad (2.63)$$

$$\frac{\partial \mathbf{u}}{\partial y}(x, y, 0) = \frac{\partial \mathbf{u}_B}{\partial y}(x, y, 0), \quad (2.64)$$

$$\frac{\partial \mathbf{u}}{\partial z}(x, y, 0) = 2 \frac{\partial \mathbf{u}_A}{\partial z}(x, y, 0) + \frac{\partial \mathbf{u}_B}{\partial z}(x, y, 0) + \mathbf{u}_C(x, y, 0). \quad (2.65)$$

Here \mathbf{u}_A , \mathbf{u}_B , and \mathbf{u}_C are the formula of the finite medium related to part A, a surface deformation related to part B, and a depth multiplied part C [17]. The deformation formula in an finite medium can be expressed by a term $\mathbf{u}_A^0(x, y, -z)$ for point source and $f^A(\varepsilon, \eta, -z) \parallel$ for finite rectangular fault source. Term $\mathbf{u}_A^0(x, y, -z)$ is refer to a function of displacement due to a point source at $(x, y, -z)$. Term $f^A(\varepsilon, \eta, -z) \parallel$ is refer to a function of displacement due to a finite rectangular source at $(\varepsilon, \eta, -z)$. Fig. 2.5 shows the result of the water surface deformation of the Indian Ocean 2004 tsunami, calculated by Okada formula.

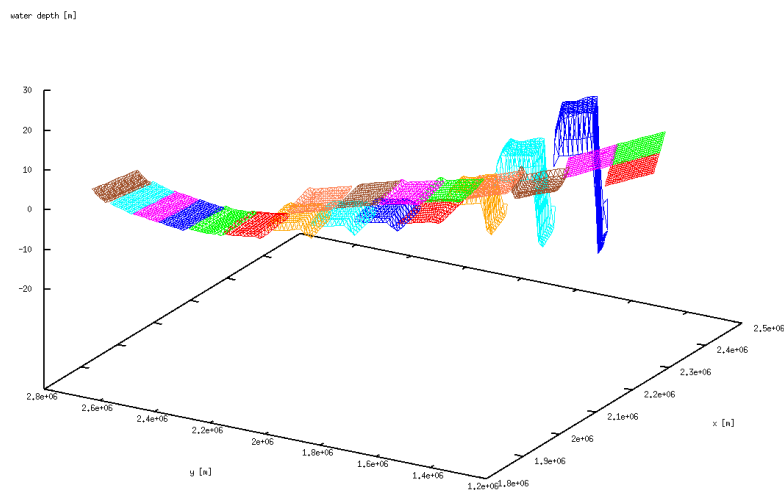


Figure 2.5: The result of water surface deformation by Okada formula.

Chapter 3

Numerical Techniques

3.1 Governing Equations

The numerical model is based on the nonlinear shallow water equations [13,22]. The following system of partial differential equations (3.1)-(3.3) were solved numerically to generate a simulation of the tsunami propagation.

$$\frac{\partial \eta}{\partial t} + \left(\frac{\partial M}{\partial x} + \frac{\partial N}{\partial y} \right) = 0, \quad (3.1)$$

$$\frac{\partial M}{\partial t} + \frac{\partial}{\partial x} \left(\frac{M^2}{H} \right) + \frac{\partial}{\partial y} \left(\frac{MN}{H} \right) + gH \frac{\partial \eta}{\partial x} + F_x = 0, \quad (3.2)$$

$$\frac{\partial N}{\partial t} + \frac{\partial}{\partial x} \left(\frac{MN}{H} \right) + \frac{\partial}{\partial y} \left(\frac{N^2}{H} \right) + gH \frac{\partial \eta}{\partial y} + F_y = 0. \quad (3.3)$$

Here, $H(x, y, t)$ is the total depth where $H(x, y, t) = h(x, y) + \eta(x, y, t)$, $z = -h(x, y)$ is sea depth and $\eta(x, y, t)$ is the water surface elevation from the mean sea level. The constant g is the gravitational acceleration. Functions $M(x, y, t)$ and $N(x, y, t)$ are the discharge fluxes, the integrations of x -component of the velocity u , and of y -component of the velocity v , respectively. Those functions is written by

$$M(x, y, t) = \int_{-h}^{\eta} u \, dz, \quad N(x, y, t) = \int_{-h}^{\eta} v \, dz. \quad (3.4)$$

Terms F_x and F_y , where

$$F_x = \frac{gn^2}{H^{\frac{7}{3}}} M \sqrt{M^2 + N^2}, \quad F_y = \frac{gn^2}{H^{\frac{7}{3}}} N \sqrt{M^2 + N^2}, \quad (3.5)$$

are the x -component and y -component of the bottom friction, respectively. The constant n is the Manning's roughness coefficient. The value of η is too small compared to h when the wave traveled in the deep sea. Thus the momentum equations become linear, due to the disregard of the nonlinear advection and bottom friction terms.

3.2 Discretization of Linearized Equations Over Triangular Mesh

Let the linearized of the system equations (3.1)-(3.3) without bottom friction terms is given by

$$\frac{\partial \eta}{\partial t} + \left(\frac{\partial M}{\partial x} + \frac{\partial N}{\partial y} \right) = 0, \quad (3.6)$$

$$\frac{\partial M}{\partial t} + g(\eta + h) \frac{\partial \eta}{\partial x} = 0, \quad (3.7)$$

$$\frac{\partial N}{\partial t} + g(\eta + h) \frac{\partial \eta}{\partial y} = 0. \quad (3.8)$$

A basis function Φ_j associated with the i^{th} node with coordinate (x_i, y_i) , is a piecewise linear function over the domain, which satisfies

$$\Phi_j(x_i, y_i) = \delta_{ij} = \begin{cases} 1 & \text{if } i = j \\ 0 & \text{if } i \neq j \end{cases}. \quad (3.9)$$

Suppose that the functions $M(x, y, t)$, $N(x, y, t)$, $\eta(x, y, t)$ and $h(x, y)$ are approximated by a linear combinations of the basis functions Φ_j .

$$M(x, y, t) = \sum_{j=1}^m M_j(t) \cdot \Phi_j(x, y), \quad (3.10)$$

$$N(x, y, t) = \sum_{j=1}^m N_j(t) \cdot \Phi_j(x, y), \quad (3.11)$$

$$\eta(x, y, t) = \sum_{j=1}^m \eta_j(t) \cdot \Phi_j(x, y), \quad (3.12)$$

$$h(x, y) = \sum_{j=1}^m h_j \cdot \Phi_j(x, y). \quad (3.13)$$

Here M_j , N_j , η_j , and h_j are unknown coefficients. The constant m is the total number of nodes.

Substituted the equations (3.10)-(3.13) into the system equations (3.6)-(3.8). Then the system equations (3.6)-(3.8) becomes

$$\sum_{j=1}^m \frac{\partial \eta}{\partial t} \Phi_j + \left(\frac{\partial M}{\partial x} + \frac{\partial N}{\partial y} \right) = 0, \quad (3.14)$$

$$\sum_{j=1}^m \frac{\partial M}{\partial t} \Phi_j + g \frac{\partial \eta}{\partial x} \sum_{j=1}^m (\eta_j + h_j) \Phi_j = 0, \quad (3.15)$$

$$\sum_{j=1}^m \frac{\partial N}{\partial t} \Phi_j + g \frac{\partial \eta}{\partial y} \sum_{j=1}^m (\eta_j + h_j) \Phi_j = 0. \quad (3.16)$$

Setting $(x, y) = (x_i, y_i)$ as for every node i , the system equations (3.14)-(3.16) becomes

$$\frac{d\eta_i}{dt} = - \left(\frac{\partial M}{\partial x} + \frac{\partial N}{\partial y} \right), \quad (3.17)$$

$$\frac{dM_i}{dt} = -g \frac{\partial \eta}{\partial x} (\eta_i + h_i), \quad (3.18)$$

$$\frac{\partial N_i}{\partial t} = -g \frac{\partial \eta}{\partial y} (\eta_i + h_i). \quad (3.19)$$

The collocation method is implemented in analysis of the system equations for discretization on a triangular mesh. Each partial derivative of the system equations (3.17)-(3.19) on the right-hand side is approximated. The approximate value of a partial derivative at each node is based on the average values of the partial derivative over the elements which share the node as a common vertex. The following equations (3.20)-(3.21) are the partial derivative at the i -th node.

$$\left(\frac{\partial \eta}{\partial x} \right)_i = \frac{1}{\sum_{k=1}^l A_k} \sum_{k=1}^l A_k \left(\frac{\partial \eta}{\partial x} \right)^{(k)}, \quad (3.20)$$

$$\left(\frac{\partial \eta}{\partial y} \right)_i = \frac{1}{\sum_{k=1}^l A_k} \sum_{k=1}^l A_k \left(\frac{\partial \eta}{\partial y} \right)^{(k)}. \quad (3.21)$$

Here A_1, A_2, \dots, A_l are the areas of the elements which share the i -th node as a common vertex. The term $\left(\frac{\partial \eta}{\partial x} \right)^{(k)}$ (Eq. 3.23) is an approximate value of the partial derivative $\left(\frac{\partial \eta}{\partial x} \right)$ at the k -th element.

3.3 Discretization of Governing Equations Over Triangular Mesh

Let $H_i = (\eta_i + h_i)$ is the total depth at node i . The discretization for the nonlinear equations (3.1)-(3.3) over a shallow water area for every node i is written as

$$\frac{d\eta_i}{dt} = - \left(\frac{\partial M}{\partial x} + \frac{\partial N}{\partial y} \right), \quad (3.22)$$

$$\frac{dM_i}{dt} = -\frac{\partial}{\partial x} \left(\frac{M^2}{H} \right) - \frac{\partial}{\partial y} \left(\frac{MN}{H} \right) - g \frac{\partial \eta}{\partial x} H_i - F_x, \quad (3.23)$$

$$\frac{dN_i}{dt} = -\frac{\partial}{\partial x} \left(\frac{MN}{H} \right) - \frac{\partial}{\partial y} \left(\frac{N^2}{H} \right) - g \frac{\partial \eta}{\partial y} H_i - F_y. \quad (3.24)$$

Here

$$F_x = \frac{gn^2}{H_i^{\frac{7}{3}}} M_i \sqrt{(M_i^2 + N_i^2)}, \quad (3.25)$$

$$F_y = \frac{gn^2}{H_i^{\frac{7}{3}}} N_i \sqrt{(M_i^2 + N_i^2)}. \quad (3.26)$$

The partial derivative on the right-hand side of the system equation (3.22)-(3.24) are approximated with

$$\frac{\partial}{\partial x} \left(\frac{M^2}{H} \right) = 2 \frac{M_i}{H_i} \frac{\partial M}{\partial x} - \frac{M_i^2}{H_i^2} \frac{\partial H}{\partial x}, \quad (3.27)$$

$$\frac{\partial}{\partial y} \left(\frac{N^2}{H} \right) = 2 \frac{N_i}{H_i} \frac{\partial N}{\partial y} - \frac{N_i^2}{H_i^2} \frac{\partial H}{\partial y}, \quad (3.28)$$

$$\frac{\partial}{\partial x} \left(\frac{MN}{H} \right) = \frac{N_i}{H_i} \frac{\partial M}{\partial x} + \frac{M_i}{H_i} \frac{\partial N}{\partial x} - \frac{M_i N_i}{H_i^2} \frac{\partial H}{\partial x}, \quad (3.29)$$

$$\frac{\partial}{\partial y} \left(\frac{MN}{H} \right) = \frac{N_i}{H_i} \frac{\partial M}{\partial y} + \frac{M_i}{H_i} \frac{\partial N}{\partial y} - \frac{M_i N_i}{H_i^2} \frac{\partial H}{\partial y}. \quad (3.30)$$

With the previous approximations, the system equations of partial differential equations (3.1)-(3.3) is reduced to a system of ordinary differential equations (ODE). The discretization of $\frac{d\eta}{dt}$ at node i expressed as

$$\frac{d\eta_i}{dt} = - \left(\frac{\partial M}{\partial x} + \frac{\partial N}{\partial y} \right), \quad (3.31)$$

while the discretization of $\frac{dM}{dt}$ at node i is given by

$$\frac{dM_i}{dt} = -\frac{\partial}{\partial x} \left[\frac{2MM_i}{H_i} - \frac{HM_i^2}{H_i^2} + g\eta H_i \right] - \frac{\partial}{\partial y} \left[\frac{MN_i}{H_i} + \frac{NM_i}{H_i} - \frac{HM_i N_i}{H_i^2} \right] - F_x, \quad (3.32)$$

and the discretization of $\frac{dN_i}{dt}$ at node i is

$$\frac{dN_i}{dt} = -\frac{\partial}{\partial x} \left[\frac{MN_i}{H_i} + \frac{NM_i}{H_i} - \frac{HM_i N_i}{H_i^2} \right] - \frac{\partial}{\partial y} \left[\frac{2NN_i}{H_i} - \frac{HN_i^2}{H_i^2} + g\eta H_i \right] - F_y. \quad (3.33)$$

Here

$$F_x = \frac{gn^2}{H_i^3} M_i \sqrt{M_i^2 + N_i^2}, \quad (3.34)$$

$$F_y = \frac{gn^2}{H_i^3} N_i \sqrt{M_i^2 + N_i^2}. \quad (3.35)$$

The system equations of ordinary differential equations (3.31)-(3.33) are solved numerically using a standard ODE solver. In this study the fourth-order Adam-Bashforth-Moulton predictor-corrector in PECE mode in conjunction with the Runge-Kutta method were employed [23].

Chapter 4

Numerical Results

4.1 Verification of the Numerical Techniques

The characteristic feature of exact solutions by Sampson et. al. [14, 15] involves moving shoreline. Consider the case where the motion of shallow water in a basin [14, 24] is governed by the equations:

$$\frac{\partial \zeta}{\partial t} + \frac{\partial(h + \zeta)U}{\partial x} + \frac{\partial(h + \zeta)V}{\partial y} = 0, \quad (4.1)$$

$$\frac{\partial U}{\partial t} + U \frac{\partial U}{\partial x} + V \frac{\partial U}{\partial y} + \tau U + g \frac{\partial \zeta}{\partial x} = 0, \quad (4.2)$$

$$\frac{\partial V}{\partial t} + U \frac{\partial V}{\partial x} + V \frac{\partial V}{\partial y} + \tau V + g \frac{\partial \zeta}{\partial y} = 0. \quad (4.3)$$

Here, $\zeta(x, y, t)$ is the height of the water surface above mean sea level, the water surface $z = -h(x, y)$ expresses the bottom surface, $U(x, y, t)$ and $V(x, y, t)$ are the depth-averaged x and y velocity components, respectively. The constant τ is the bottom friction parameter, and constant g is the gravity acceleration. Consider the flow takes place in the parabolic canal:

$$h(x, y) = h_0 \left(1 - \frac{x^2}{a^2}\right), \quad (4.4)$$

where $h = 0$ and a are positive constants.

The exact solutions for $\tau < \sqrt{\frac{8gh_0}{a^2}}$ are given by:

$$U(x, y, t) = B e^{-\frac{\tau t}{2}} \sin(st), \quad (4.5)$$

$$V(x, y, t) = 0, \quad (4.6)$$

$$\zeta(x, y, t) = \zeta_0(x, y, t) + x \zeta_1(x, y, t), \quad (4.7)$$

where

$$\zeta_0(x, y, t) = \frac{a^2 B^2 e^{-\tau t}}{8g^2 h_0} \left[-s\tau \sin(2st) + \left(\frac{\tau^2}{4} - s^2 \right) \cos(2st) \right] - \frac{B^2 e^{-\tau t}}{4g}, \quad (4.8)$$

$$\zeta_1(x, y, t) = \left[\frac{e^{-\frac{\tau t}{2}}}{g} \left(Bs \cos(st) + \frac{\tau B}{2} \sin(st) \right) \right]. \quad (4.9)$$

Here,

$$s = \frac{\sqrt{p^2 - \tau^2}}{2}$$

and

$$p = \sqrt{\frac{8gh_0}{a^2}}$$

. The numerical techniques of the finite element analysis were applied to the equations (4.1)-(4.3), and yields:

$$\frac{\partial \zeta}{\partial t} = -\frac{\partial \zeta}{\partial t} u + \frac{2h_0 x}{a^2} u, \quad (4.10)$$

$$\frac{\partial u}{\partial t} = -\left(\tau u + g \frac{\partial \zeta}{\partial x} \right), \quad (4.11)$$

$$\frac{\partial v}{\partial t} = -g \frac{\partial \zeta}{\partial y}. \quad (4.12)$$

To obtain the numerical results, initial conditions (4.13)-(4.15) were set.

$$u(t_0) = B e^{-\frac{\tau t_0}{2}} \sin(st_0), \quad (4.13)$$

$$v(t_0) = 0, \quad (4.14)$$

$$\zeta(t_0) = \zeta_0(t_0) + x \zeta_1(t_0), \quad (4.15)$$

where

$$\zeta_0(t_0) = \frac{a^2 B^2 e^{-\tau t_0}}{8g^2 h_0} \left[-s\tau \sin(2st_0) + \left(\frac{\tau^2}{4} - s^2 \right) \cos(2st_0) \right] - \frac{B^2 e^{-\tau t_0}}{4g}, \quad (4.16)$$

$$\zeta_1(t_0) = \left[\frac{e^{-\frac{\tau t_0}{2}}}{g} \left(Bs \cos(st_0) + \frac{\tau B}{2} \sin(st_0) \right) \right]. \quad (4.17)$$

The exact solution and a numerical solution were considered in a parabolic canal which has constants value $a = 3$ km, $h_0 = 10$ m for motion in which $B = 5$ m s^{-1} . The exact solutions which compared with the numerical results are the exact solutions obtained for $\tau = 0.001$ s^{-1} [14].

Fig. 4.1 (a) and (b) show profile of the initial water surface for a numerical solution and exact solution, respectively. The comparison of the water surface profiles between a numerical result and the exact solutions at the first 800 seconds are illustrated. Fig. 4.2 (a) shows the comparison of the water surface movement at the time $t = 200$ seconds. Fig. 4.2 (b)-(d) show the comparison of the water surface movement at the time $t = 400$ seconds, $t = 600$ seconds, and $t = 800$ seconds, respectively. The comparison between exact solutions and numerical results shows an acceptable agreement for every time step for the first 800 seconds. However, numerical results for water elevation ζ start to increase enormously around the water surface boundaries and become uncontrollable.

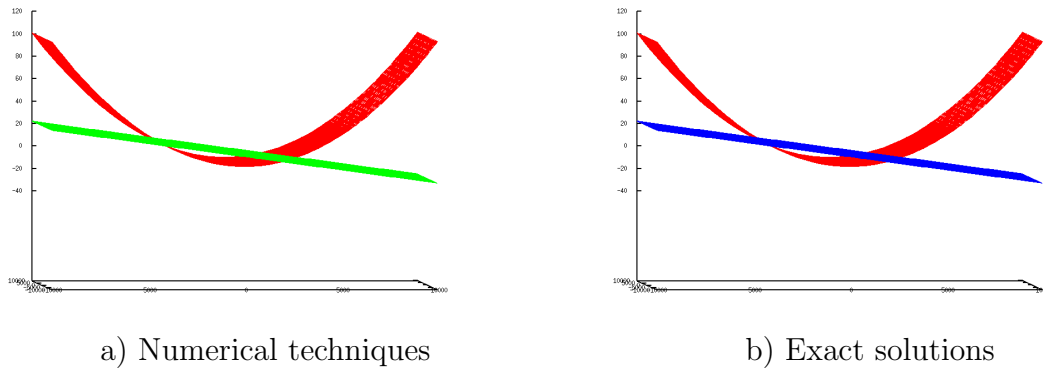
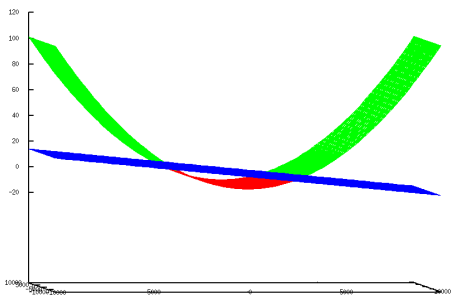
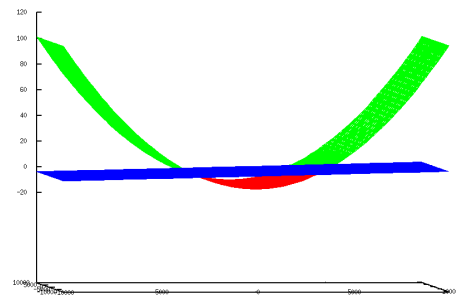


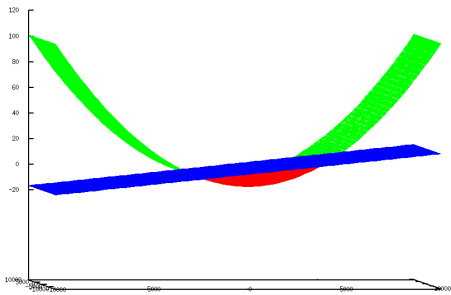
Figure 4.1: Profiles of the initial water surface.



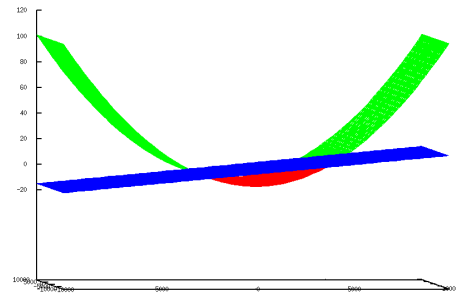
a) $t = 200$ sec.



b) $t = 400$ sec.



c) $t = 600$ sec.



d) $t = 800$ sec.

Figure 4.2: Comparison of the water surface movement between numerical techniques (Green) and exact solutions (Blue).

Chapter 5

Numerical Simulation of Tsunami Propagation

5.1 The Algorithm of The Simulation

The simulation process consists of eight steps.

1. Collecting the bathymetry data.

In this case, obtained data is the complete data set gives global coverage on a one arc-minute grid. An arc-minute is a unit of the angular measurement which is equal to $\frac{1}{60}$ of one degree. A minute of arc is $\frac{1}{21600}$ of a turn or $\frac{\pi}{10800}$ of a radian. The data is in the form of 2D (two-dimensional) netCDF data sets (.nc). Each file consists of two sections, the CF header and the data section. The CF header is split into a number of components; dimensions, variables and global attributes. The data section is the section contains the actual values for each dimension and variable. The data values represent elevation in metres, with negative values for bathymetric depths and positive values for topographic heights.

```

Global Attributes:
  Conventions = 'CF-1.0'
  title       = 'The GEBCO One Minute Grid - a continuous terrain model for oceans and land at one arc-minute intervals'
  institution = 'On behalf of the General Bathymetric Chart of the Oceans (GEBCO) the data are held at the British Oceanographic Data Cen
source       = 'The grid is largely based on the bathymetric contours contained in the GEBCO Digital Atlas (GDA) with existing gridded d
history      = 'This is version 2.0 of the data set, released in November 2008'
references   = 'Information on the data set is available from the internet: http://www.gebco.net/data_and_products/gridded_bathymetry_da
comment      = 'The data in the GEBCO One Minute Grid should not be used for navigation or any purpose relating to safety at sea.'
node_offset  = 0
History      = 'Translated to CF-1.0 Conventions by Netcdf-Java CDM (NetcdfCFWriter)
              Original Dataset = /local/webassdata/grid/gebco/GRIDONE_2D_301381.nc; Translation Date = Wed Sep 14 03:26:01 BST 2016'

Dimensions:
  lat = 1261
  lon = 1261

Variables:
  elevation
    Size:      1261x1261
    Dimensions: lon,lat
    Datatype:  int16
    Attributes:
      long_name = 'Elevation relative to sea level'
      units     = 'm'
      scale_factor = 1
      add_offset = 0
      actual_range = [-10577 8430]
      coordinates = 'lat lon '

  lat
    Size:      1261x1
    Dimensions: lat
    Datatype:  double
    Attributes:
      standard_name = 'latitude'
      long_name     = 'latitude'
      units         = 'degrees_north'
      axis          = 'Y'
      _CoordinateAxisType = 'Lat'

  lon
    Size:      1261x1
    Dimensions: lon
    Datatype:  double
    Attributes:
      standard_name = 'longitude'
      long_name     = 'longitude'
      units         = 'degrees_east'
      axis          = 'X'
      _CoordinateAxisType = 'Lon'

```

Figure 5.1: An example of the 2D netCDF data sets display.

2. The Matlab is used to convert the 2D netCDF data sets into the latitude, longitude, and elevation data values.
3. The Gauss-Krugër projection is applied for conversion of the curvilinear coordinates into the Cartesian coordinates with a C programming.
4. A triangular mesh over the topographical domain is generated and yields numbers of nodes and elements which used in the discretization of the model. The process consists the numbering of the nodes and the elements .
5. The topographical feature is generated with a C programming and visualized.
6. Okada formulation [16,17] is used to calculation the water surface displacement. The calculation based on Okada model is required nine parameters of the source fault plane. Those parameters are the latitude, longitude, length, width, and depth of the source fault plane. Moreover, the strike angle, the rake angle, the dip angle, and the slip amount distribution of the source fault plane also inputted into the calculation. A C programming has been used. The calculated water surface displacement is set as the initial water surface displacement for the tsunami wave generation. Thus the initial water surface displacement is visualized.

7. The calculation of the numerical solutions and the simulation of the tsunami wave propagation are obtained by using a programming. The numerical solutions consists of the wave heights elevation per time simulation (second).
8. The graphical visualization of the numerical solutions is generated with AVS/Express data visualization toolkit.

Those previous steps are repeated for both cases simulation, the Mentawai 2010 tsunami and the Indian Ocean 2004 tsunami.

5.2 Simulation of the Mentawai 2010 Tsunami

Topographical data of the Mentawai Islands regency were stretched from 85.0°E to 106.0°E and 6.0°N and 15.0°S. Those data were obtained from British Oceanographic Data Centre (BODC), General Bathymetric Chart of the Oceans (GEBCO) in form of One Minute Grid (GRIDONE) [25]. A C programming has been used to simulate the tsunami wave for a rectangular domain of 1260 sub-rectangles in the x -direction and 1260 sub-rectangles in the y -direction. Each sub-rectangle was further divided into 2 triangles. A triangular mesh of the Mentawai 2010 tsunami simulation has 1,590,121 total nodes and 3,175,200 total elements.

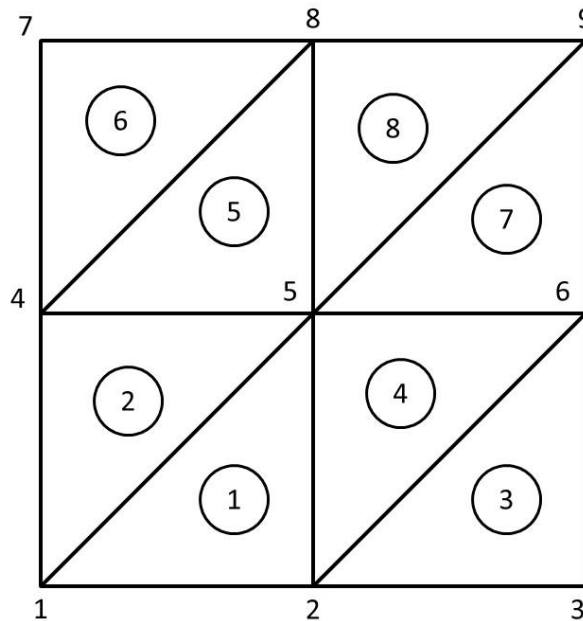


Figure 5.2: The illustration of the nodes and the elements numbering process.

The initial water surface displacement based on Okada [16, 17] was set. A source fault plane lie at 99.86567°E to 100.10976°E and 2.55268°S to 4.34144°S. Nine parameters of source fault planes were obtained from Satake, et.al [6]. The source fault plane were divides into 28 sub-faults with 30 km length and 30 km width. The dip angle was set to 7.5° for sub-faults with depth 2-5.92 km and 12° for sub-faults with depth 9.83-16.07 km.

The strike angle and rake angle were set to 326° and 101° , respectively. The slip amount distribution ranged from 0.0 m and 6.10 m. The results of the calculation show that the water height of surface displacement were range to 0 m to 3 m. The maximum water surface displacement up to 3 m (sub-fault 4) appeared near Pagai islands.

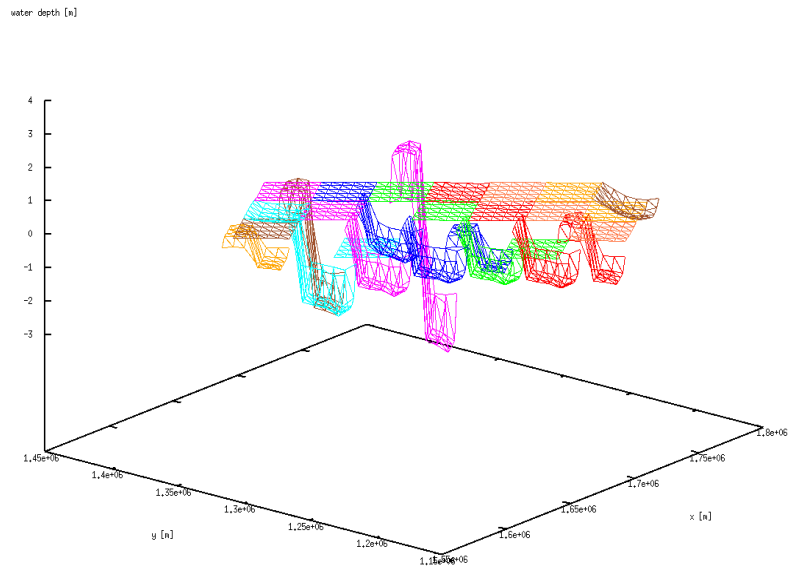


Figure 5.3: The initial water surface displacement of 28 sub-faults [29].

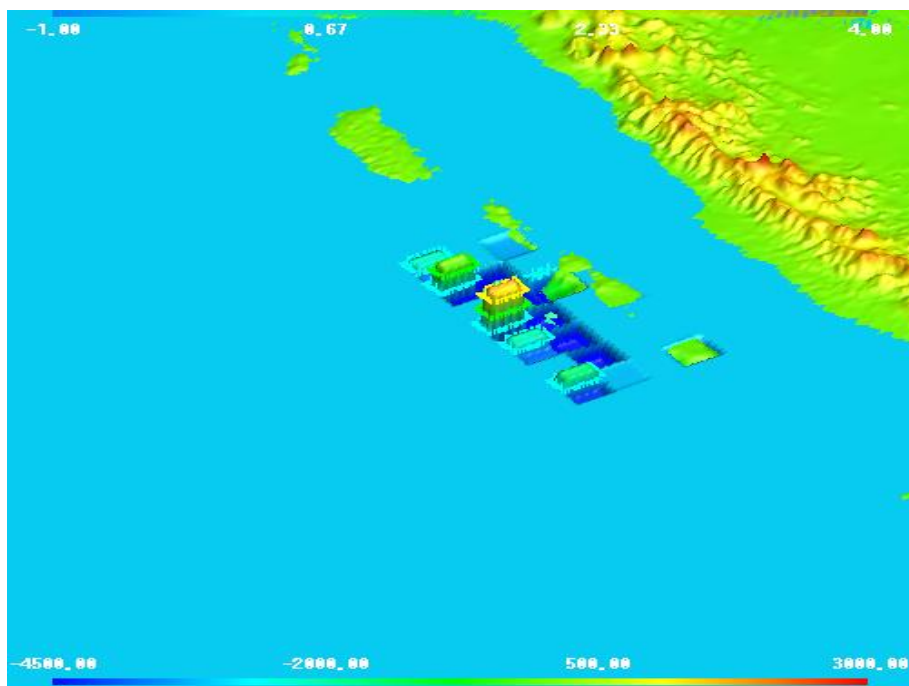


Figure 5.4: The simulation of the initial water surface displacement.

The propagation of the Mentawai 2010 tsunami for 5100 seconds or for the first 85 minutes was simulated. The initial water surface displacement for the simulation was set (Fig. 5.4). The initial wave was collapsed and reached shoreline area at the time prior to 600 seconds or from the first 10 min. after the earthquake. Mikami et.al. [26] stated that the first tsunami wave arrived at 10-20 min. after the earthquake occurred. The arriving time of our numerical results also similar to the confirmation by the eye-witnesses [27], which stated that the first wave reached shoreline area at 5-15 min. after the earthquake. The Indonesia Meteorological Climatological, and Geophysical Agencies (BMKG) issued a national warning for a local tsunami five minutes after the earthquake [6].

The simulation of the Mentawai 2010 tsunami was illustrated in the figures below. Fig. 5.5 (a) shows the tsunami wave propagation at the time of up to 15 minutes. In this phase, the initial wave reached the shoreline areas of the Mentawai Islands regency. The Pagai islands were the first part of the Mentawai Islands which were attacked by tsunami wave. The next part of the Mentawai Islands which was hit by tsunami wave was Siberut island, as shown in Fig. 5.5 (b). It happened for the last 30 minutes of simulation, and there was a small ripples that reached the shoreline area of the Sumatra Island. Fig. 5.5 (b)-(f) show the propagation of the tsunami wave for the time up to 45 minutes, 60 minutes, 75 minutes, and the last 85 minutes, respectively.

The numerical results yields the maximum wave height is up to 3 m and occurred at the shoreline of the South Pagai Island (Fig. 5.6) at the time greater than 2000 seconds. Tsunami waves up to 2 m also occurred at the shoreline of the South Pagai island. The tsunami wave height at several points in the Mentawai Islands regency were observed. Those points are at Sipora Island, Malakopa, Simagandjo and Tua Pejat. The Sipora Island area was reached by greater than 1 m of the tsunami wave. A tsunami wave with height up to 3 m was appeared at the Malakopa, South Pagai Islands. There are no significant water surface displacement occurred at the Simagandjo, North Pagai and at the capital city of the Mentawai Islands regency, Tua Pejat. Fig. 5.7 and Fig. 5.8 show the wave height changes at Sipora Islands and South Pagai Islands. The highest wave at the observed point in the Sipora Islands was greater than 1.5 m at the Sipora area. The average wave height at those observed points were ± 0.5 m. At the same time, the maximum wave height changes at the observed points in the South Pagai islands occurred at Malakopa. The wave height changes at the Beleratsok and Sibigau Island were ± 1 m, while no wave height change at Tiop, Bulasat, and Sibigau island were observed.

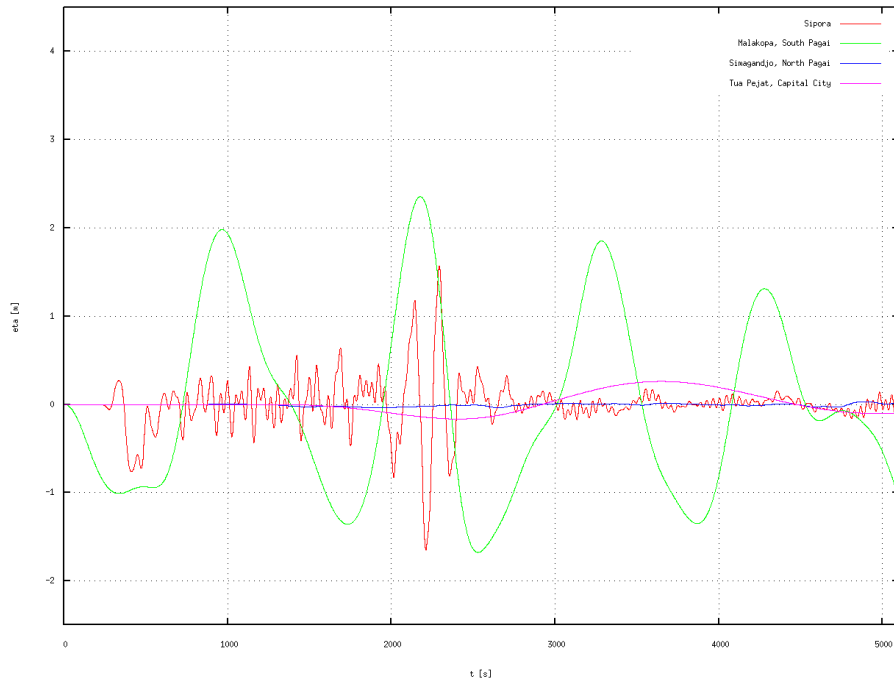


Figure 5.6: Wave height changes at several points in the Mentawai Islands regency.

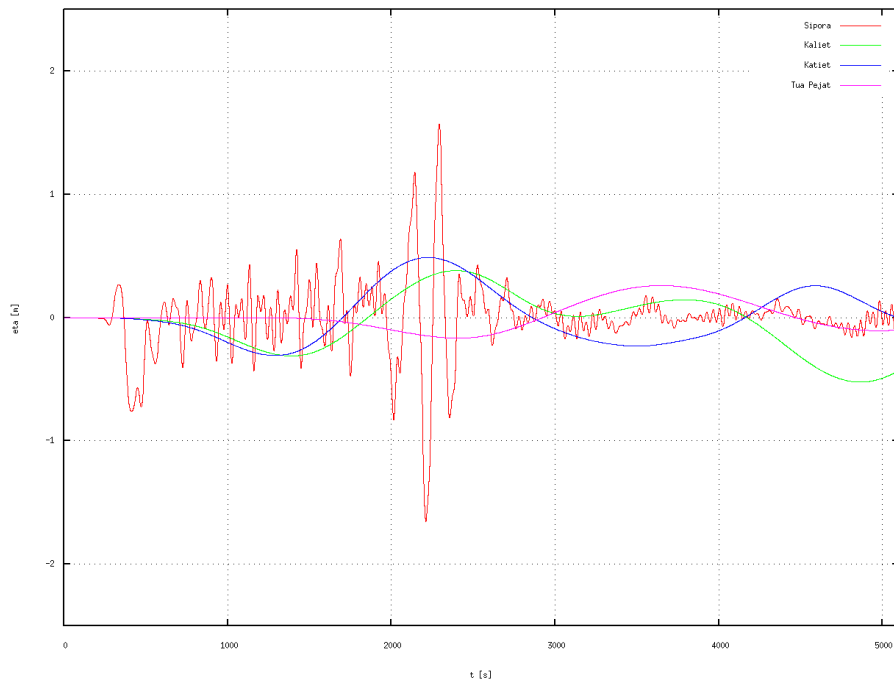


Figure 5.7: Wave height changes at Sipora islands in the Mentawai Islands regency.

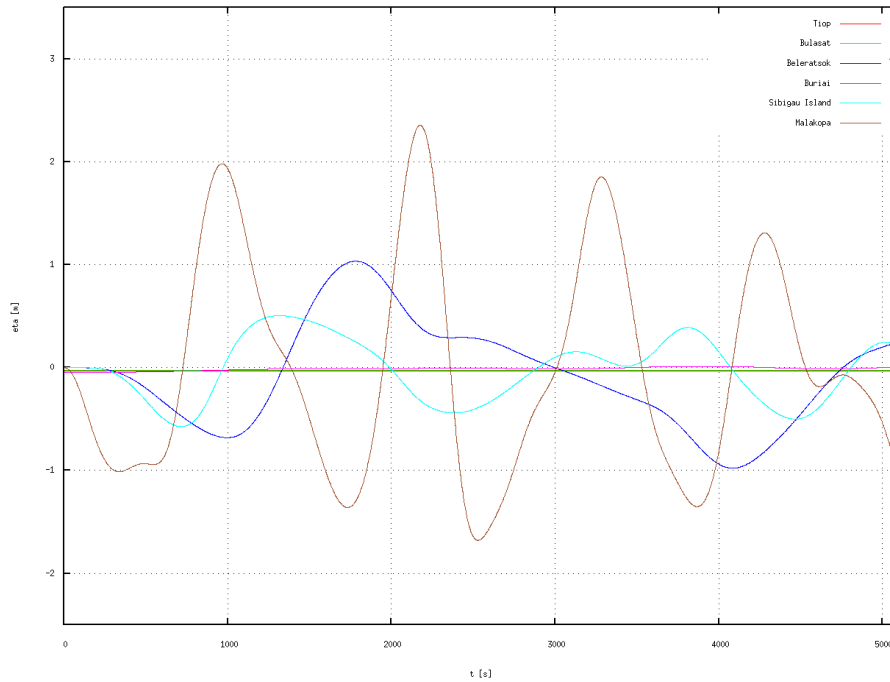


Figure 5.8: Wave height changes at South Pagai islands in the Mentawai Islands Regency.

Fig. 5.9, 5.10 and 5.11 show the comparison between numerical results and gauge station data. Tide gauge station data were obtained from the United Nations Educational, Scientific and Cultural Organization (UNESCO), Intergovernmental Oceanographic Commission (IOC), Sea Level Station Monitoring Facility website [28]. Those data were collected by the time 21:42 WIB (Western Indonesia Time) to 23:12 WIB. Three tide gauge station at the vicinity of the Mentawai Islands regency were chosen. Those station are Tanahbala station which located at 98.5°E and 0.53°N , Teluk Dalam station which located at 97.822°E and 0.554°S , and Enggano station which located at 102.2781°E and 5.3461°N . This results also mentioned in [29, 30].

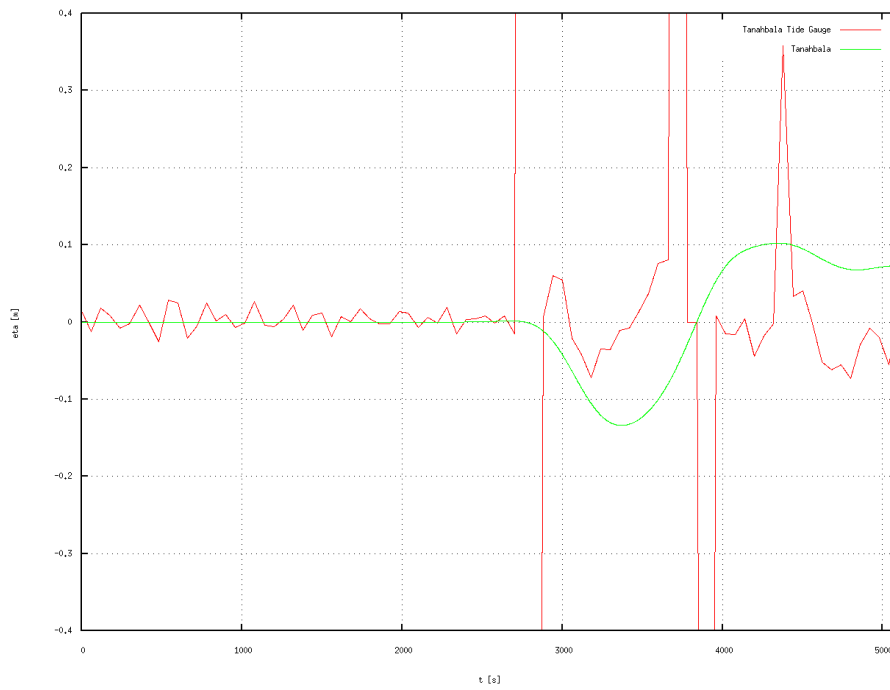


Figure 5.9: Wave changes comparison between the Tanahbala station (red) and numerical results (green).

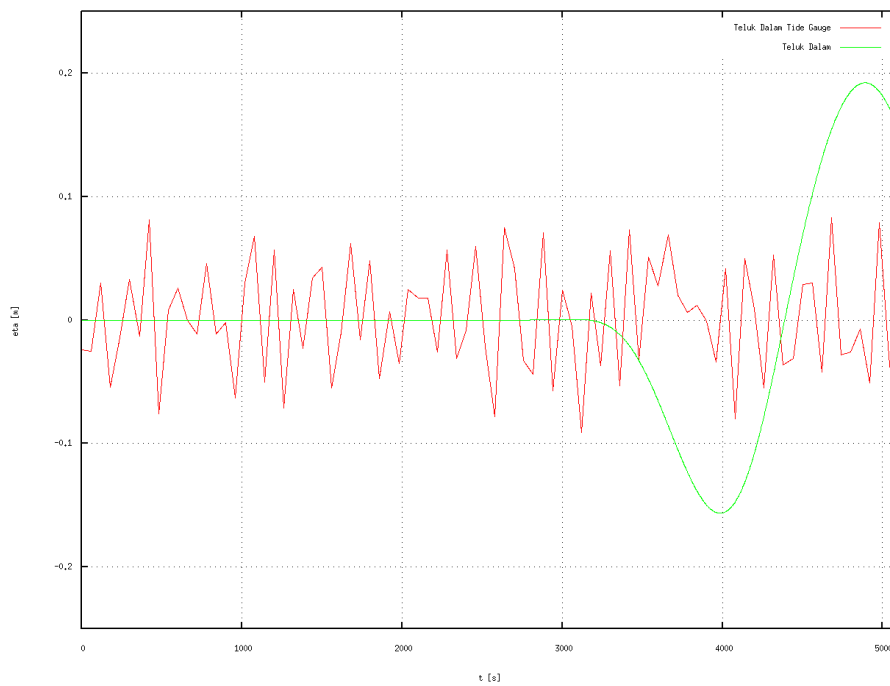


Figure 5.10: Wave changes comparison between the Teluk Dalam station (red) and numerical results (green).

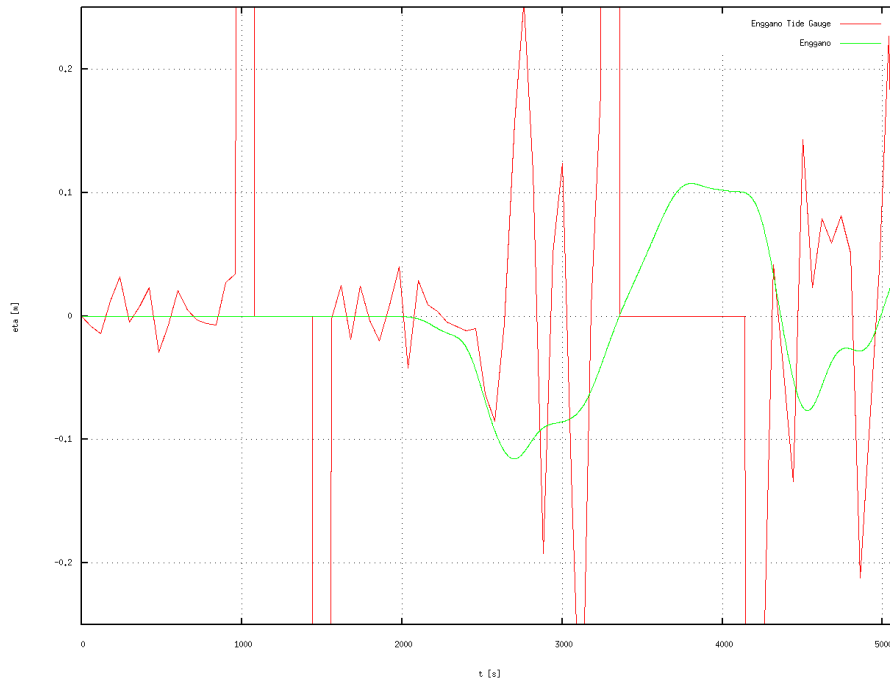


Figure 5.11: Wave changes comparison between the Enggano station (red) and numerical results (green).

5.3 Simulation of the Indian Ocean 2004 Tsunami

Topographical data of the Indian Ocean 2004 tsunami were stretched from 75.0°E to 103.0°E and 10.0°N and 18.0°S [23]. The simulation of the tsunami wave consist a rectangular domain with 1680 sub-rectangles in the x -direction and 1680 sub-rectangles in the y -direction. Each sub-rectangle was divided into 2 triangles. A triangular mesh of the Indian Ocean 2004 tsunami simulation has 2,825,761 total nodes and 5,644,800 total elements. The initial water surface displacement [16,17] was generated for an initial condition. The source fault plane of the Indian Ocean tsunami 2004 consisting 22 sub-faults. It stretched from 91.51°E to 96.23°E and 1.75°N and 13.51°N . The dip angle was set to 10° , the strike angle ranged from 0° to 350° , and the rake angle ranged from 85° to 130° . The value of the slip amount distribution ranged from 0.1 m to 30.3 m [5]. The numerical results based on Okada formulation [16,17] showed that the maximum water surface displacement was approximately 20 m. Fig. 5.12 shows the initial water surface displacement of the Indian Ocean 2004 tsunami simulation.

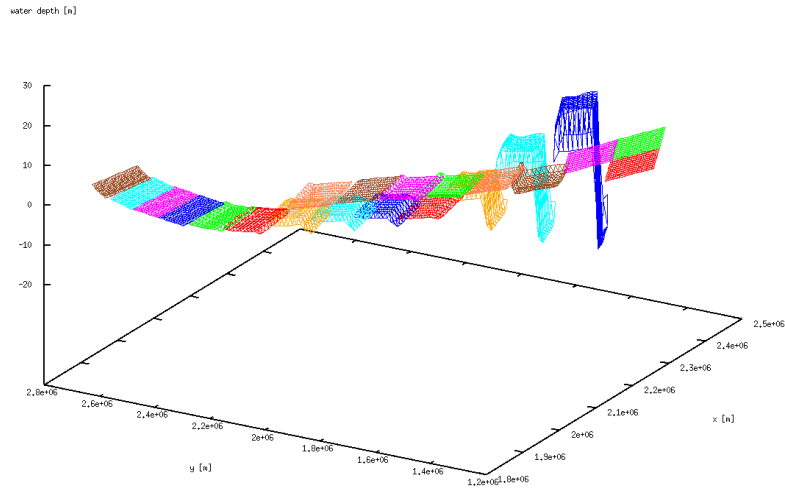


Figure 5.12: The initial water surface displacement of 22 sub-faults [30].

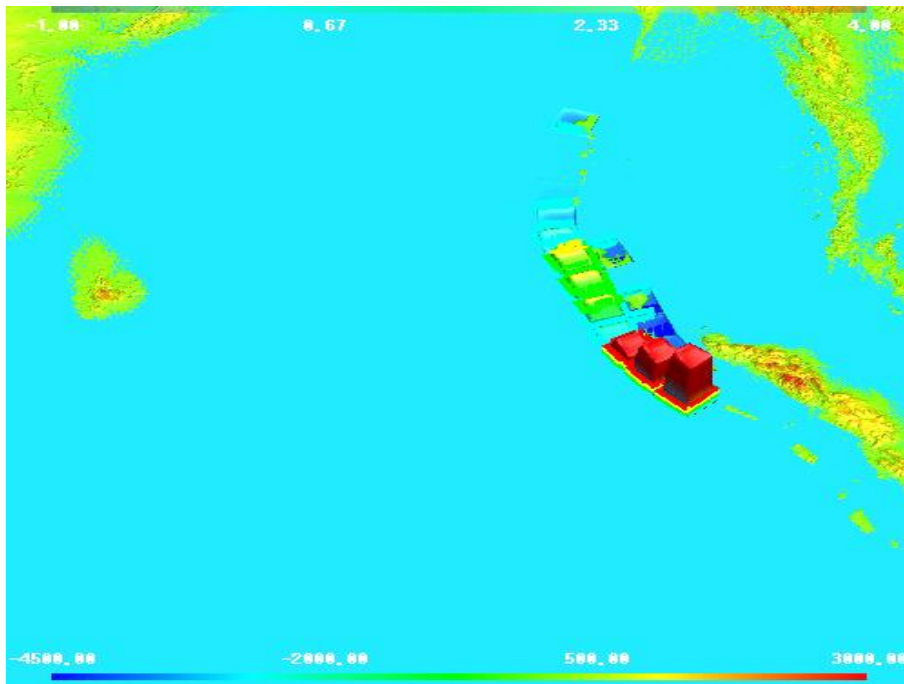


Figure 5.13: The initial water surface displacement of the Indian Ocean 2004 tsunami.

The propagation of the Indian Ocean 2004 tsunami for the first 3600 seconds or 1 hour was simulated. The initial waves were collapsed and approached shoreline area of Aceh province after five to fifteen minutes. The study by Syamsidik et. al. [10] reported the arriving times of tsunami waves at the several areas in Aceh province, Indonesia. The tsunami wave reached Sabang area twenty two minutes after the earthquake, while

Banda Aceh area was reached at the time 35 min. after the earthquake. The tsunami wave reached the Lageun, Calang, and Teunom Aceh Jaya at the time 25-62 min., 29-72 min., and 29-72 min., respectively. The tsunami wave reached the Tapaktuan, South Aceh 24-37 min. after the earthquake. The tsunami wave reached Singkil at the fifty three minutes after the earthquake.

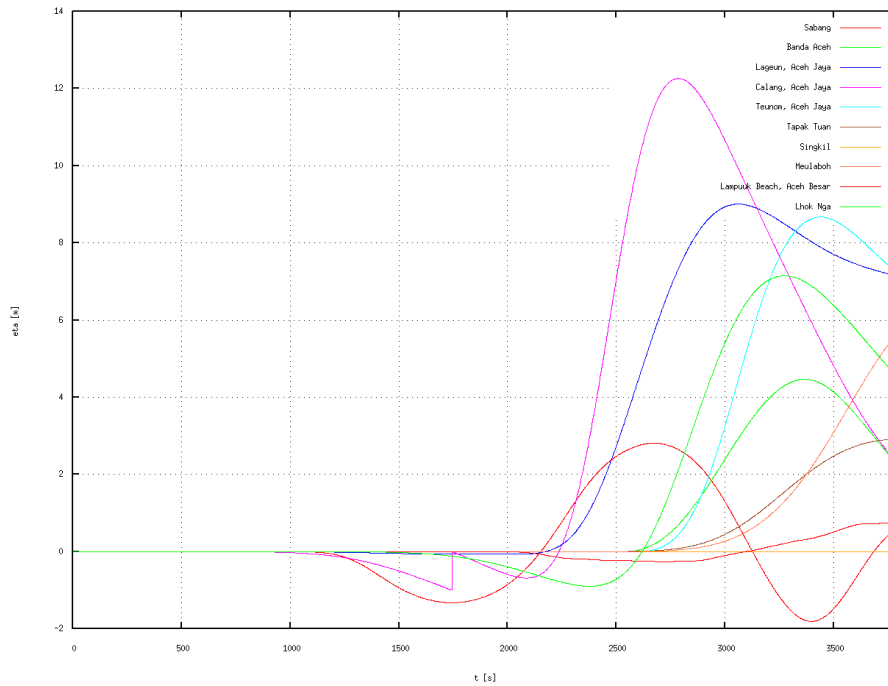


Figure 5.14: Wave height changes at several points in Aceh province, Indonesia.

Fig. 5.14 shows numerical results the wave height changes at several points in the Aceh province, Indonesia. Fig. 5.15, Fig. 5.16, Fig. 5.17, and Fig. 5.18 show that the arriving time of tsunami waves at Banda Aceh after 41 minutes, Lampuuk beach after 25 minutes, Aceh Jaya after 33 minutes, and Sabang after 16 minutes after the earthquake. Meanwhile, tsunami waves approached the shoreline area of Lhok Nga at 33 min. after the earthquake (Fig. 5.19). Tsunami waves reached the shoreline area of Tapaktuan and Meulaboh at the first 42 min. in Fig. 5.20 and Fig. 5.21, respectively.

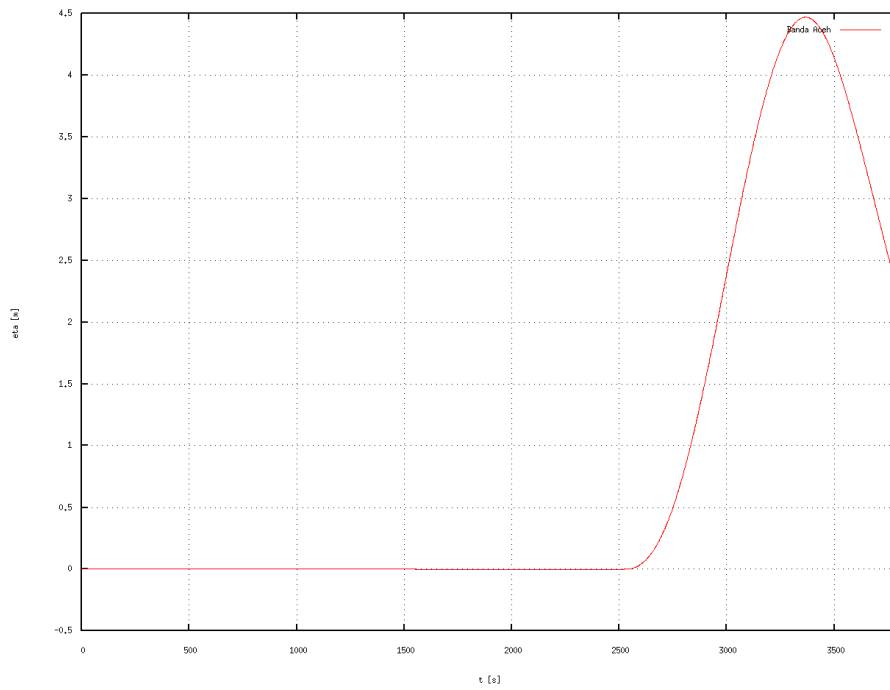


Figure 5.15: Wave height transition at Banda Aceh in the Aceh province, Indonesia.

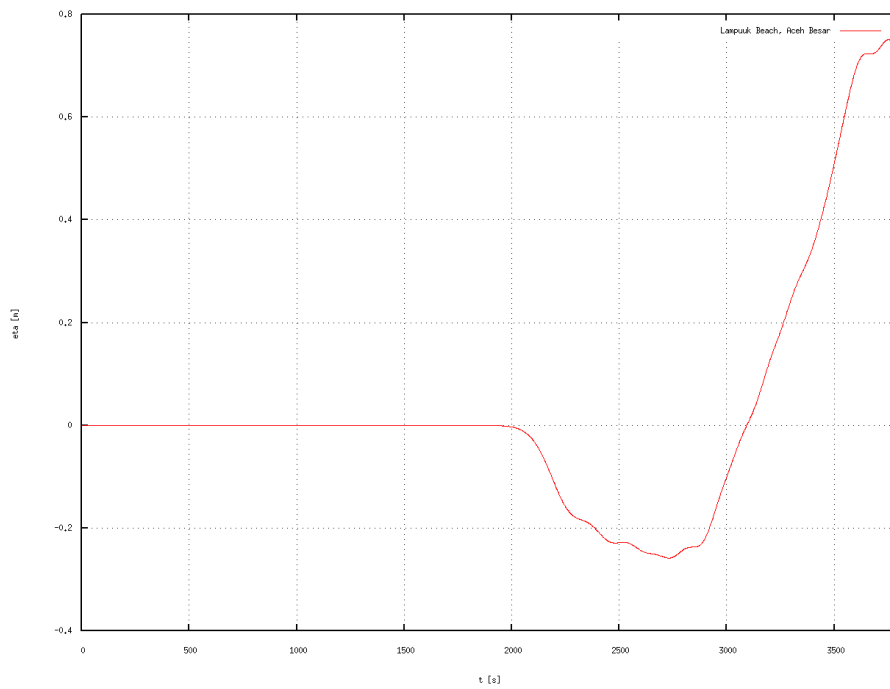


Figure 5.16: Wave height transition at Lampuuk beach in the Aceh province, Indonesia.

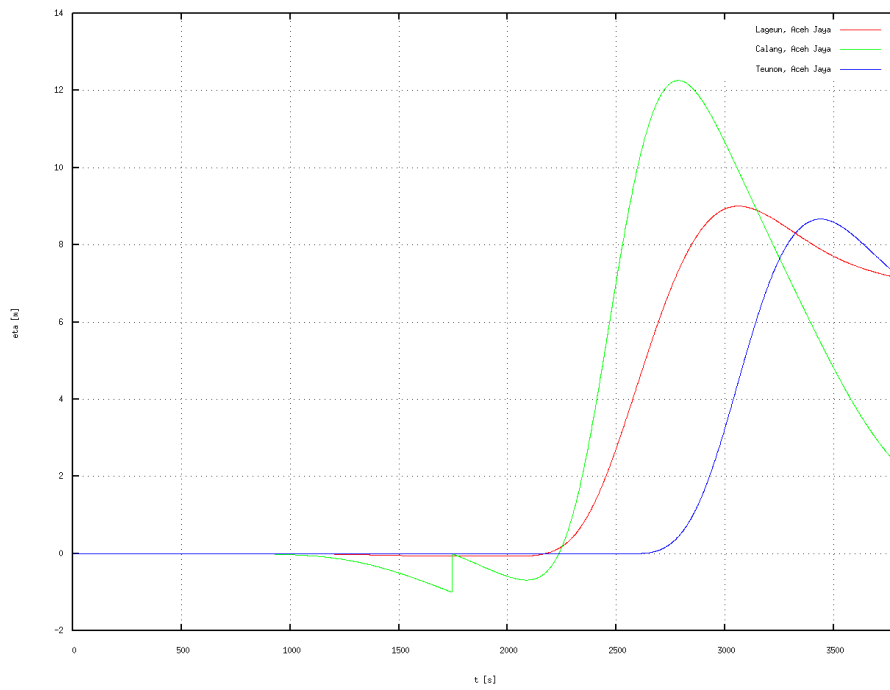


Figure 5.17: Wave height transition at Aceh Jaya, Aceh province, Indonesia.

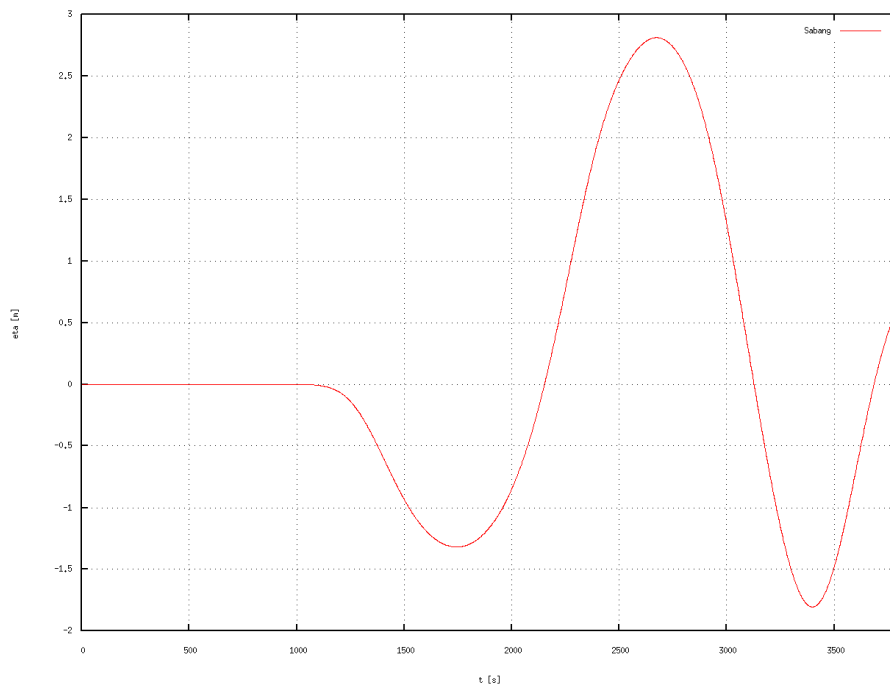


Figure 5.18: Wave height transition at Sabang in the Aceh province, Indonesia.

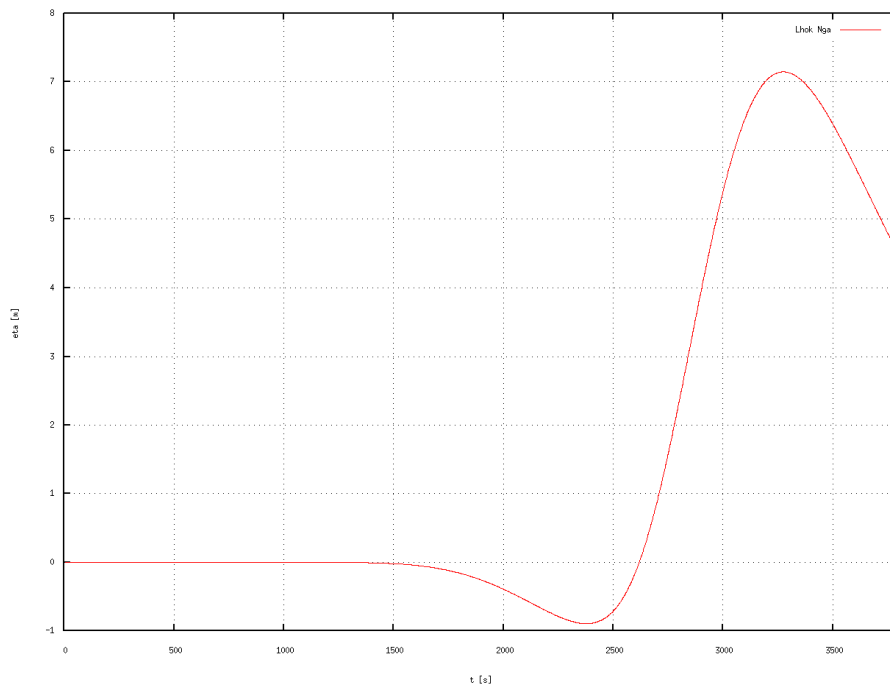


Figure 5.19: Wave height transition at Lhok Nga in the Aceh province, Indonesia.

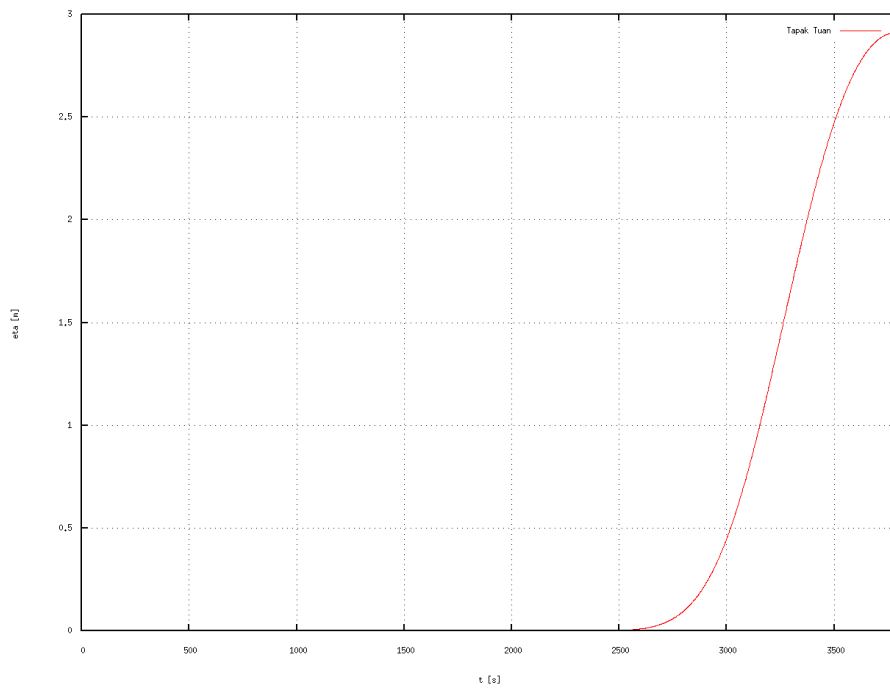


Figure 5.20: Wave height transition at Tapaktuan in the Aceh province, Indonesia.

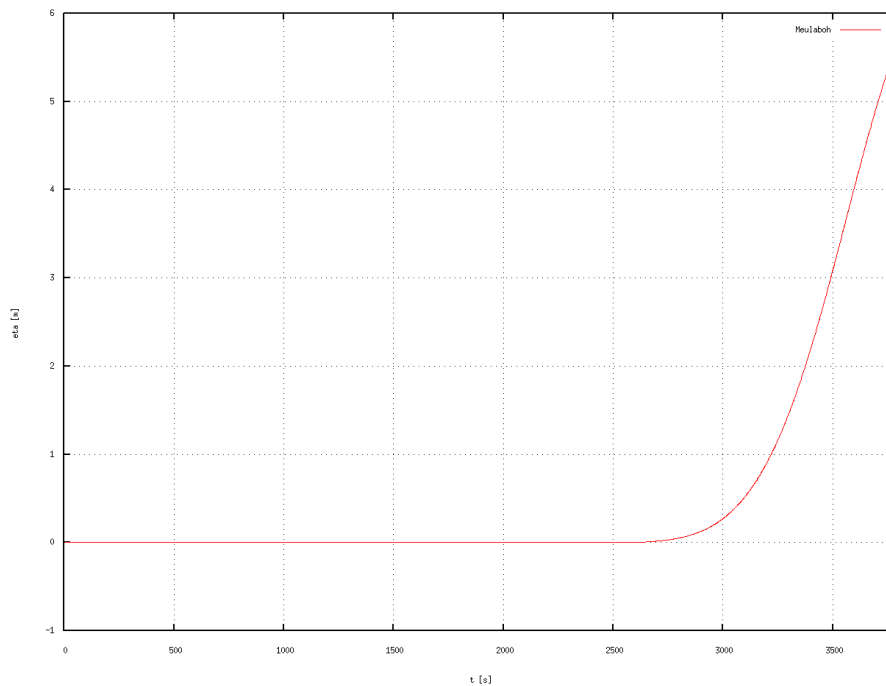
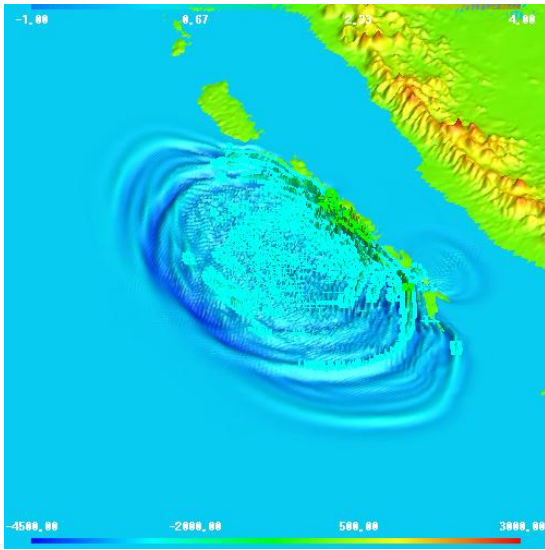
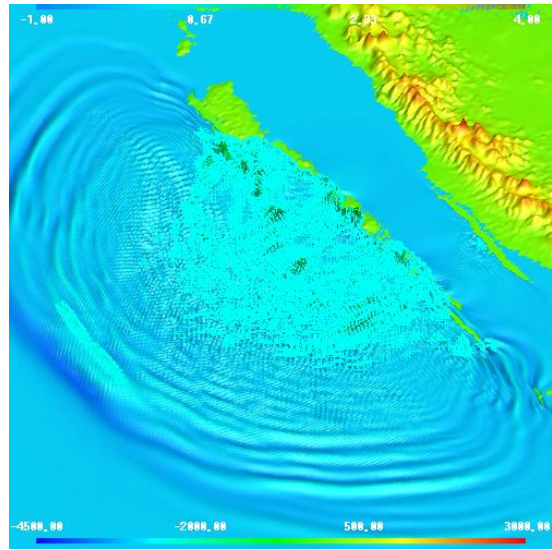


Figure 5.21: Wave height transition at Meulaboh in the Aceh province, Indonesia.

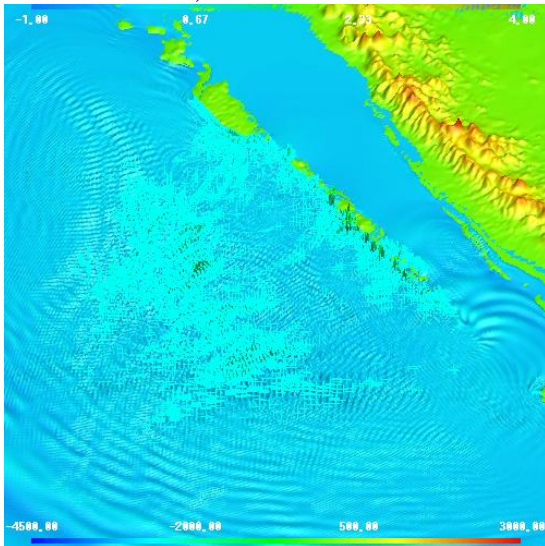
Fig. 5.12 shows the numerical results of the water surface displacement of the Indian Ocean 2004 tsunami. Fig. 5.13 shows that most of the source fault plane were generated in the vicinity area of the Aceh Province sea. Three sub-faults with the maximum water surface displacement were generated at the west coast of Aceh Province. Fig. 5.22 (a)-(f) show tsunami wave propagation of the Indian Ocean 2004 tsunami. Profiles of the tsunami wave at the time 10 minutes, 20 minutes, 30 minutes, 40 minutes, 50 minutes, and 60 minutes was illustrated. The maximum wave height for the numerical simulation was reset to 30 m, that is, the wave height was set equal to 30 m when it exceeds 30 m. These results also mentioned in [29, 30].



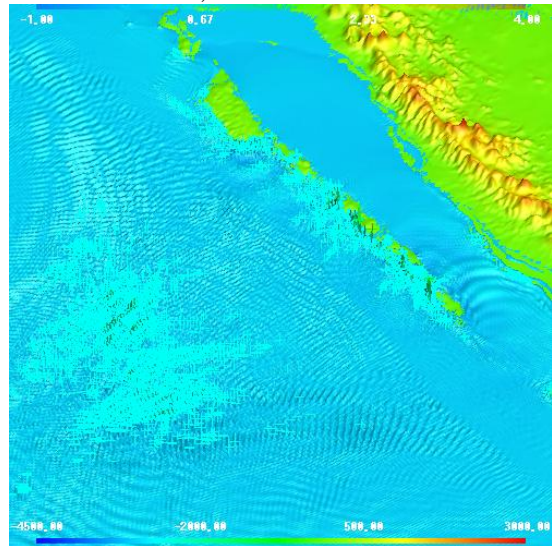
a) $t = 15$ min.



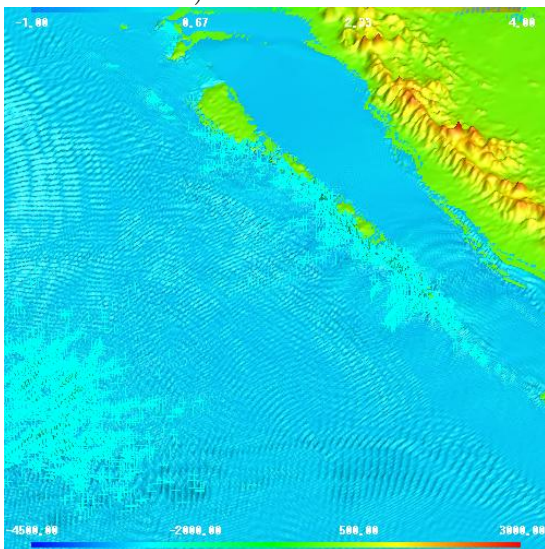
b) $t = 30$ min.



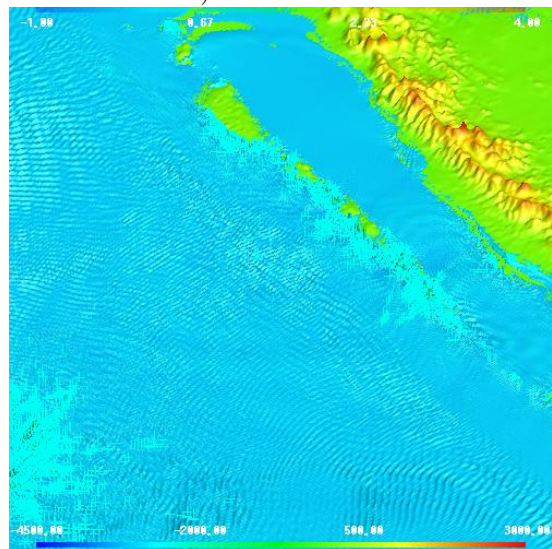
c) $t = 45$ min.



d) $t = 60$ min.

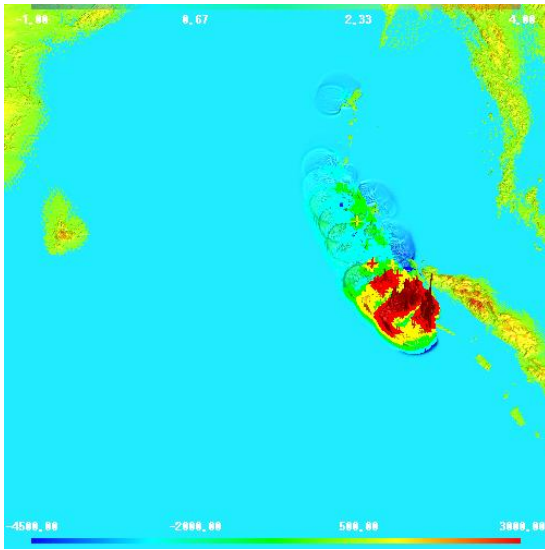


e) $t = 75$ min.

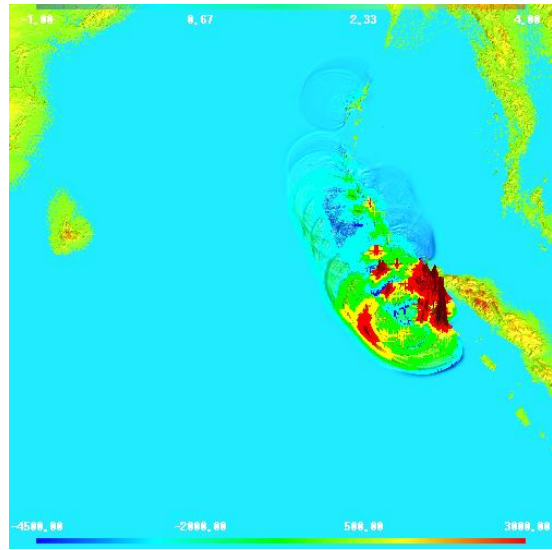


f) $t = 85$ min.

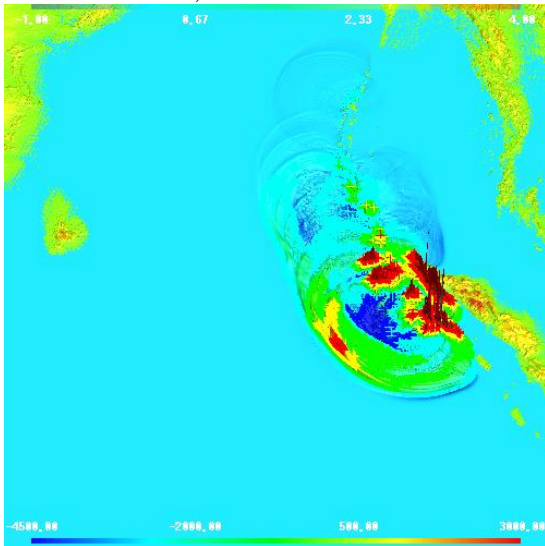
Figure 5.5: Tsunami wave propagation of the Mentawai 2010 tsunami.



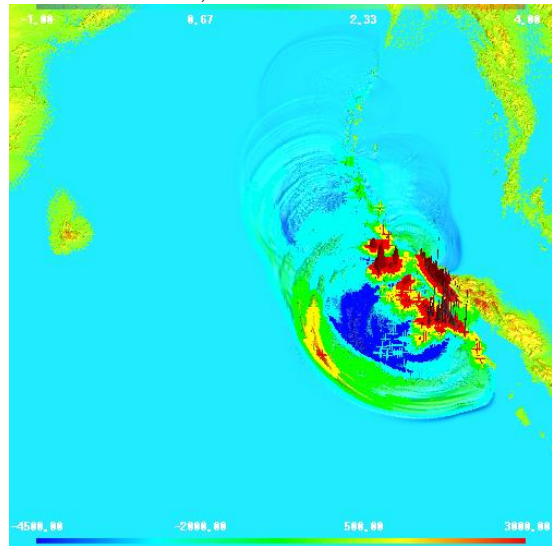
a) $t = 10$ min.



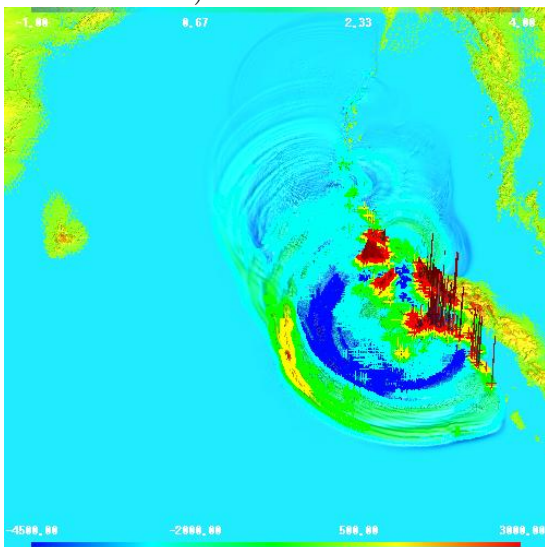
b) $t = 20$ min.



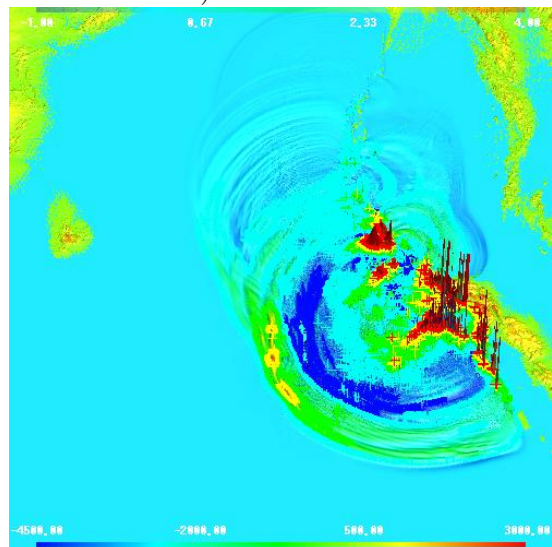
c) $t = 30$ min.



d) $t = 40$ min.



e) $t = 50$ min.



f) $t = 60$ min.

Figure 5.22: Tsunami wave propagation of the Indian Ocean 2004 tsunami [30].

Chapter 6

Conclusion and Future Research

6.1 Conclusions

The simulation of the Mentawai 2010 tsunami and the Indian Ocean 2004 tsunami was illustrated. The simulation was generated in conjunction with the application of moving shoreline techniques. Our numerical results were tested against the exact solutions of the two-dimensional nonlinear shallow water equations for flow above parabolic bottom topography. The comparison shows an acceptable agreement between our numerical techniques and the exact solutions for approximately the first 800 seconds. Numerical results of the water elevation became increase enormously around the boundary area. However, the uncontrollability did not appear in the simulation of the Mentawai 2010 data and the Indian Ocean 2004 data.

The propagation of tsunami waves of the Mentawai 2010 tsunami were simulated for the first 85 minutes after the earthquake. The source fault plane was divided into 28 sub-faults. The maximum water surface elevation was up to 3 m and located at the west side of the Pagai islands. The numerical results show that the initial waves collapsed and reached the shoreline area of the Mentawai islands in approximately ten minutes after the earthquake. Tsunami wave height at several points in the Mentawai islands were observed and illustrated in the figures. Three tide gauge station data were compared with the numerical results. The maximum wave height up to 3 m appeared at the shoreline area of the South Pagai Island.

Tsunami waves propagation of the Indian Ocean 2004 tsunami were simulation for one hour after the earthquake. Twenty two sub-faults were generated from the nine parameters source fault plane data. Three highest water surface displacement of the twenty two sub-faults were generated in the west coast of the Aceh province, Indonesia. The maximum water surface displacement was up to 20 m. The simulation show that the initial waves ruptured and approached the shoreline area of the Aceh province at the first 5-50 min. after the earthquake. Several points at the Aceh province were observed and their wave height were illustrated in the figures. The maximum wave height was set to 30 m and appeared at the several points in the Aceh coast area. Tsunami wave with height up to 3 m was appeared in the shoreline of the Aceh province, Indonesia.

6.2 Future Research

The future research will be conducted to investigate the comparison between numerical results and exact solutions. The uncontrollability of the numerical solutions at the time after 800 seconds will be tackled for flow above parabolic bottom topography. The refinement of a triangular mesh will be applied for improvement of numerical approximation. The results obtained will be used as a basic framing for the system of the tsunami early warning. Those results will also be used as a basis planning for the tsunami hazard assessment. Another tsunami event cases will be considered.

Bibliography

- [1] E. Guidoboni, J. E. Ebel, Earthquakes and Tsunamis in the past: A guide to techniques in historical seismology, Cambridge University Press, 2009.
- [2] <http://www.walrus.we.usgs.gov/tsunami.basic.html>
- [3] <https://www.ngdc.noaa.gov/hazard/tsu.shtml>
- [4] <https://earthquake.usgs.gov/earthquakes/>
- [5] Y. Fujii, K. Satake, Tsunami source of the 2004 Sumatra-Andaman earthquake inferred from tide gauge and satellite data, *Bulltein of the Society of America*, vol. 97, no. 1A, pp. S192-S207, Jan. 2007.
- [6] K. Satake, Y. Nishimura, P. S. Putra, A. R. Gusman, H. Sunendar, Y. Fujii, Y. Tanioka, H. Latief, E. Yulianto, Tsunami source of the 2010 Mentawai, Indonesia earthquake inferred from Tsunami field survey and waveform modeling, *Pure Applied Geophysics*, vol. 170, pp. 1567-1582, 2013.
- [7] B. Poisson, C. Oliveros, R. Pedreros, Is there a best source model of the Sumatra 2004 earthquake for simulating the consecutive tsunami?, *Geophysical Journal International*, vol. 185, pp. 1365-1378, 2011.
- [8] K. D. Chule, K. K. Ok, C. B. Ho, K. K. Hwan, E. Pelinovsky, Three-dimensional runup simulation of the 2004 Indian Ocean tsunami at the Lhok Nga twin peaks, *Journal of Coastal Research*, Special Issue no. 65, 2013.
- [9] Y. Tanioka, Yudhicara, T. Kususose, S. Kathiroli, Y. Nishimura, S-I. Iwasaki, K. Satake, Rupture process of the 2004 great Sumatra-Andaman earthquake estimated from tsunami waveforms, *Earth Planets Space*, vol. 58, pp. 203-209, 2006.
- [10] Syamsidik, T. M. Rasyif, S. Kato, Development of accurate tsunami estimated times of arrival for tsunami-prone cities in Aceh, Indonesia, *International Journal of Disaster Risk Reduction*, vol. 14, pp. 403-410, 2015.
- [11] E. Ulutas, Tsunami simulation of the October 25, 2010, South Pagai Island, Sumatra earthquake, *International Journal of the Physical Sciences*, vol 6, no. 3, pp. 459-475, 2011.
- [12] E. Ulutas, A. Inan, A. Annunziato, Web-based tsunami early warning system: a case study of the 2010 Kepulauan Mentawai earthquake and tsunami, *Natural Hazards and Earth System Sciences*, vol. 12, pp. 1855-1871, 2012.

- [13] F. Imamura, A. C. Yalciner, G. Ozyurt, Tsunami modelling manual (TUNAMI model), IUGG/IOC Time Project, IOC MAnuals and Guides No. 35, UNESCO, 1997.
- [14] J. Sampson, A. Easton, M. Singh, Moving boundary shallow water flow above parabolic bottom topography, ANZIAM J. 47 (EMAC 2005), pp. C373-C387, 2006.
- [15] J. Sampson, A. Easton, M. Singh, A new moving boundary shallow water wave equation numerical model, ANZIAM J. 48 (CTAC 2006), pp. C605-C617, 2007.
- [16] Y. Okada, Surface deformation due to shear and tensile faults in a half-space, Bulletin of the Seismological Society of America, vol. 75, no. 4, pp. 1135-1154, 1985.
- [17] Y. Okada, Internal deformation due to shear and tensile faults in a half-space, Bulletin of the Seismological Society of America, vol. 82, no. 2, pp. 1018-1040, 1992.
- [18] R. Wait, A. R. Mitchell, Finite element analysis and applications, John Wiley Sons, Great Britain, 1986.
- [19] J. N. Reddy, An introduction to the finite element method, McGraw-Hill Book Company, 1984.
- [20] R. E. Deakin, M. N. Hunter, C. F. F. Karney, The Gauss-Krugër projection, The Victorian Regional Survey Conference, Warrnambool, 2010.
- [21] 山本和弘, 船体動揺による誤差の補正を考慮した三次元水底地形データの計測と有限要素メッシュ上のデータ更新, Okayama University, March, 2013.
- [22] Y. Otani, K. Yamamoto, Hashentuya, M. Watanabe, Numerical study of the effects of tsunamis using a finite element method, ANZIAM J. 52 (CTAC2010), pp. C1031-C1048, 2011.
- [23] J. D. Lambert, Computational methods in ordinary differential equations, John Wiley Sons, Great Britain, 1979.
- [24] C. B. Vreugdenhil, Numerical methods for shallow-water flow, Kluwer Academic Publisher, The Netherlands, 1998.
- [25] British Oceanographic Data Center (BODC), Natural Environmental Research Council, General Bathymetric Chart of the Ocean (GEBCO), <https://www.bodc.ac.uk/>.
- [26] T. Mikami, T. Shibayama, M. Esteban, K. Ohira, J. Sasaki, T. Suzuki, H. Achiari, T. Widodo, Tsunami vulnerability evaluation in the Mentawai islands based on the field survey of the 2010 tsunami, Natural Hazards, vol. 71, pp. 851-870, 2014.
- [27] E. M. Hill, J. C. Borrero, Z. Huang, Q. Qiu, P. Banerjee, D. H. Natawidjaja, P. Elosegui, H. M. Fritz, B. W. Suwargadi, I. R. Pranantyo, L. li, K. A. Macpherson, V. Skanavis, C. E. Synolakis, K. Sieh, The 2010 M_w 7.8 Mentawai earthquake: very shallow source of a rare tsunami earthquake determined from tsunami field survey and near-field GPS data, Journal of Geophysical Research, vol. 117, 2012.

- [28] United Nations Educational, Scientific and Cultural Organization (UNESCO), Inter-governmental Oceanographic Commission (IOC), Sea Level Station Monitoring Facility, <http://www.ioc-sealevelmonitoring.org/>.
- [29] N. Alfiany, K. Yamamoto, M. Watanabe, Numerical study of tsunami propagation in Mentawai Island West Sumatra, *Universal Journal of Geoscience*, vol. 5, no. 4, pp. 112-116, 2017.
- [30] N. Alfiany, M. Watanabe, Application of numerical techniques to tsunami propagation, *Proceeding of the Seventh International Conference on Advance in Civil, Structural and Environmental Engineering*, 2018.